# Role of Nickel Doping on Magnetocaloric Properties of La0.7Sr0.3Mn1-xNixO3 Manganites

**Selda Kılıç Çetin** ( kilics@cu.edu.tr )

Central Research Laboratory, Çukurova University, Adana, Turkey https://orcid.org/0000-0003-4112-4475

**Gönül Akça**

Cukurova University: Cukurova Universitesi

**Mehmet Selim Aslan**

Cukurova University: Cukurova Universitesi

**Ahmet Ekicibil**

Cukurova University: Cukurova Universitesi

**Original Research**

**Keywords:** Magnetocaloric effect, Manganites, Magnetic entropy change, Landau theory, Curie temperature

**Posted Date:** February 4th, 2021

**DOI:** https://doi.org/10.21203/rs.3.rs-164109/v1



**Version of Record:** A version of this preprint was published at Journal of Materials Science: Materials in Electronics on March 20th, 2021. See the published version at https://doi.org/10.1007/s10854-021-05702-2.

# Role of Nickel doping on magnetocaloric properties of $La_{0.7}Sr_{0.3}Mn_{1-x}Ni_xO_3$ manganites

Selda Kılıç Çetin[a]*, Gönül Akça[b], Mehmet Selim Aslan[b] and Ahmet Ekicibil[b]

[a]*Central Research Laboratory, Çukurova University, Adana, Turkey.*
[b]*Department of Physics, Faculty of Sciences and Letters, Çukurova University, Adana, Turkey.*

**Abstract:**

This study reports the effect of Ni substitution for Mn on structural, magnetic and magnetocaloric properties of $La_{0.7}Sr_{0.3}MnO_3$ manganite synthesized by sol-gel technique. The structural, morphological and magnetic properties are investigated using x-ray diffractometer (XRD), scanning electron microscope (SEM) and vibrating sample magnetometer (VSM) systems. XRD results showed that all samples crystallize in rhombohedral structure. Thermomagnetic measurements showed that $T_C$ decreases with the addition of Ni from 363 K for x = 0.00 to 324 K for x = 0.06. $\Delta S_M$ determined by Maxwell's relations and Landau theory gave compatible results in the transition temperature and region above. $\Delta S_M^{max}$ values were determined as 4.52, 4.51, 4.41 and 3.90 $Jkg^{-1}K^{-1}$ for x = 0.00, 0.02, 0.04 and 0.06 at 5T, respectively. The Arrott plots and the scaling analysis of $\Delta S_M$, which collapsed on a single curve, showed that magnetic transitions are second order.

**Keywords:** Magnetocaloric effect, Manganites, Magnetic entropy change, Landau theory, Curie temperature.

***Corresponding Author:**
Dr. Selda Kılıç Çetin
Central Research Laboratory,
Çukurova University, 01330 Adana, Turkey
e-mail: kilics@cu.edu.tr

## 1. Introduction

Because of global warming and climate change, our dependence on air conditioning and cooling systems is increasing day by day to improve our living standards. This situation causes an enhancement of energy consumption in these areas. Energy consumption must keep under control for the development of countries in all areas. Therefore, countries have to make regulations and they study to improve new systems with low energy consumption. Among the existed and studied cooling and air conditioning systems, magnetic refrigeration (MR) systems have been quite hopeful because of high energy efficiency and low energy consumption [1] when compared to conventional gas compression systems extensively using in all areas. These systems have quite good properties environmentally [2]. In addition, these systems are also low cost and noise [3]. MR systems work according to magnetocaloric effect (MCE). Briefly, this effect is defined as the temperature change of a magnetic material under magnetic field [2]. Except of refrigeration, the MCE has been drawn interest for the conversion and harvesting of the energy [4] and medical area (such as drug delivery and hyperthermia) [5].

Magnetic entropy change ($\Delta S_M$) and adiabatic temperature ($T_{ad}$) change are two magnitudes which are defining the MCE [6]. All magnetic materials show magnetocaloric (MC) properties because of being an internal property of the materials [7]. The basic purpose of the studies on the MCE is to provide the appropriate cooling element for MR systems [5, 8, 9]. The MC materials have to meet certain requirements in order to be used in MR applications [2, 3]. Since the discovery of the MCE, it has been identified different families of materials that may be suitable for MR systems [8-14]. Among of these material families, $RE_{1-x}A_xMnO_3$ perovskite manganites (where RE states rare earth elements and A points out monovalent or divalent elements) have investigated intensively for their physical properties [15-20]. The physical properties of manganite materials affect by several factors such as sample production method, chemical stoichiometry and the type of metal ion [21]. The type of metal ion replaced by the A or Mn site changes the double exchange (DE) interaction. Consequently, this affects the magnetic and MC properties of the samples. There are some studies showing the effect of element replacing such as Co, Cr, Cu, and Ni by Mn on magnetic and MC properties [21-25]. In these studies, it is aimed to obtain materials that can be used as candidate refrigerant material for MR systems.

One of the perovskite manganite family, La-based $La_{0.7}Sr_{0.3}MnO_3$ compound has been attracted quite due to its high magnetic phase transition temperature and high colossal magnetoresistive value [26]. To improve the physical properties and attain deep information of $La_{0.7}Sr_{0.3}MnO_3$ compound, the $La_{0.7}Sr_{0.3}MnO_3$ compound has been prepared by using different

techniques [26-28]. Furthermore, by making dopings/substitutions to both of A and B-site, the effects on physical properties have been investigated [23, 24, 26, 27, 29-31]. This study reports the effect of Ni-doped $La_{0.7}Sr_{0.3}Mn_{1-x}Ni_xO_3$ ($0 \leq x \leq 0.06$) manganites prepared by sol-gel technique on the structural, magnetic and MC properties.

## 2. Experimental Procedure

$La_{0.7}Sr_{0.3}Mn_{1-x}Ni_xO_3$ ($0.00 \leq x \leq 0.06$) manganite samples abbreviated as LSM, LSM2, LSM4 and LSM6, respectively, have been produced by sol-gel technique. To synthesize the sample, $La(NO_3)_3.6H_2O$, SrO, NiO and $Mn(NO_3)_2.6H_2O$ compounds are used. The processes of the sol-gel method are given in the previous studies [32]. To obtain the samples targeted, stoichiometric ratios of the initial materials firstly were solved in optimum solvents. The solutions were mixed by the magnetic stirrer at a certain temperature. To obtain gel form, auxiliary chemicals were added to the solutions in appropriate proportions. To obtaining the dried form, the samples were heated on a hot plate. The final samples were calcined 600 ℃ for 6 h. The sintering temperature and time for the sample is 1200℃ and 24 h, respectively. The structural properties and grain structure of the samples were investigated by using x-ray diffractometer (XRD) with a PANalytical-EMPYREAN diffractometer and scanning electron microscope (SEM) using a FEI-Quanta 650 Field Emission microscope. To identify the magnetic properties and compute the value of $\Delta S_M$ for the samples, magnetization measurements vs. temperature ($M(T)$) and magnetic field ($M(H)$) were performed by using physical properties measurement systems (PPMS) with a vibrating sample magnetometer (VSM) option of Quantum Design PPMS DynaCool-9. The *M(T)* measurements were performed at the temperature interval between 5-380K under a magnetic field of 10mT. After determining the magnetic phase transition temperature of the samples, the *M(H)* measurements were made with 4K temperature increments in the transition temperature range up to 5T.

## 3. Results and Discussions

Figures 1(a-d) show the XRD spectra taken at room temperature for $La_{0.7}Sr_{0.3}Mn_{1-x}Ni_xO_3$ ($0.00 \leq x \leq 0.06$) manganites. As seen from the figure, the diffraction patterns of all samples are similar to each other, and it observed that there is no detectable secondary phase. The diffraction peaks were indexed in the rhombohedral structure. Lattice parameters and unit cell volume of the samples are specified by using Fullprof software and these values are given

in Table 1. As seen from Table 1, the unit cell volume of the samples decreases with increasing Ni concentration. This decreasing may be explained by $Ni^{2+}$ ionic radius (0.55 Å) is smaller than $Mn^{3+}$ (0.65 Å) one. Even though the unit cell volume and lattice parameters change with $Ni^{2+}$ content, no change in crystal structure was observed. These changes in the structural properties of the samples are expected to cause variation in the magnetic and MC properties of the compounds. The structural results obtained in this study are similar to the literature [33, 34].

Manganites are found in perovskite structure and it is controlled by equation formulized with $t = (r_A + r_O)/\sqrt{2}(r_{Mn} + r_O)$ is known as tolerance factor ($t$). It is a dimensional criterion that depends on the sizes of the ions and characterizes the distinct structures derived from the perovskite structures. In the equation, the ionic radii of the A cation, B cation and oxygen are represented by $r_A$, $r_B$ and $r_O$, respectively. The values of $r_A$ and $r_B$ are given in the Table 1. In ideal perovskites $t$ is equal to one and crystal structure is cubic. But, the crystal structure of the materials covaries with the changing of the $t$ value. [35]. For rhombohedral structure, $t$ values are between 0.96 and 1.0 [36]. By using Shannon's Table [37], we have calculated the average radii of A and B-sites as well as $t$ value and these values are given in Table 1. The $t$ value for the samples increases with increasing Ni ratio in the system from 0.9792 for x = 0.00 to 0.9812 for x = 0.06. When Ni is added instead of Mn, according to the neutrality equation ($La^{3+}_{0.7}Sr^{2+}_{0.3}Mn^{3+}_{0.7-x}Mn^{4+}_{0.3+x}Ni^{2+}_{x}O^{2-}_{3}$) [38], $Mn^{3+}$ decreases while $Mn^{4+}$ increases. In case, it is occurred that a decrease in the average ionic size of the B- site. As result, the average ionic size of B site decrease and the $t$ values increase. The calculated $t$ values affirm that the crystal structure of the samples is rhombohedral.

Morphological properties of the samples affect the magnetic and MC properties of the samples. Therefore, the morphology of the samples was investigated using SEM at 20 KX magnifications. The SEM images of the samples are given in the Fig.2. From SEM images, it is seen that grains have slightly different sizes and polygonal volume particle structures, mostly spherical and the grain boundary is clear for all samples. The grain sizes of the samples are calculated by using Image J software and are seen in Table 1. The histograms of the grain size are given in Fig. 3. It is observed that the grain size is reduced with increasing Ni concentration.

The elemental analyzes of the samples were performed using SEM with equipment energy dispersive x-ray spectroscopy (EDS). Figure 4 shows the EDS spectra of the samples. All elements seen from EDS peak reflections belong to the elements that form the samples. The peak reflection of any element other than the compounds used in the sample production process was not scanned. In addition, it can be seen from the EDS spectra that the number and intensity of Ni peaks increase in proportion to the increase in Ni concentration. Atomic percentages of

the elements that compose the compound according to the results of the EDS analysis are given in Table 2. According to the chart, it is seen that the elements forming the compounds do not suffer any loss during production.

Thermomagnetic measurements were carried out to study the magnetic behavior of $La_{0.7}Sr_{0.3}Mn_{1-x}Ni_xO_3$ ($0.00 \leq x \leq 0.06$) samples and to determine their transition temperatures. Figure 5 shows the zero-field cooling (ZFC) and field-cooling (FC) magnetization curves in the temperature range 5-380 K under 10 mT. From the magnetization curves, it is seen that the samples change from the ferromagnetic (FM) to the paramagnetic (PM) with increasing the temperature. As thermal interaction energy increases with the increase of temperature the FM coupling is disrupted and consequently magnetization rapidly decreases to zero at a temperature. This temperature called as Curie temperature ($T_C$). As seen in figure, while the ZFC and FC curves overlap in the PM region, it is seen that the curves diverge when moving towards the FM region. Since the highest separation is observed in the LSM4 sample, we can say that the most anisotropy is in this sample. Another situation that confirms the high anisotropy of this material is that the magnetization increases as the temperature decreases in the FC curve. In cases where anisotropy is low, the magnetization value follows a constant path with temperature decrease. The $T_C$ values of the samples were determined as 363, 351, 344 and 324 K for LSM, LSM2, LSM4 and LSM6, respectively. From the results, it is seen that $T_C$ decreases as the amount of Ni replaced by Mn increases. Ni doping in the Mn region causes an increase in the number of ions from the $Mn^{3+}$ state to the $Mn^{4+}$ state. The transformation of the $Mn^{3+}$ ($t^3_{2g}$, $e^1_g$) ion to the $Mn^{4+}$ ($t^3_{2g}$, $e^0_g$) state is defined as the hole (space) doping [39]. The $Mn^{4+}$ / $Mn^{3+}$ ratio formed with the addition of Ni to the structure was calculated as 0.43, 0.48, 0.55 and 0.62 for LSM, LSM2, LSM4 and LSM6, respectively. Thus, it can be said that with the increase of Ni amount, a decrease in the $T_C$ is observed due to the decrease in the number of conduction electrons. In addition, newly formed $Mn^{3+}$- O -$Ni^{2+}$, $Mn^{4+}$- O - $Mn^{4+}$ and $Ni^{2+}$- O - $Ni^{2+}$ bond interactions that will weaken the FM double exchange interactions and support the antiferromagnetism with the substitution of Mn by $Ni^{2+}$ ions [34]. As a result, the $T_C$ gradually decreases as the amount of Ni increases.

After the determination of the $T_C$ temperatures, isothermal magnetization measurements were taken in this temperature region in order to determine the $\Delta S_M$, which are mostly changing in this region. The *M(H)* measurements were carried out in the $T_C$ region in 4K temperature steps up to 5T applied magnetic field and are shown in Fig. 6 for the samples. As can be seen clearly from the Fig. 6, *M(H)* curves leading to the saturation particular to FM state at low

temperatures, while they are in the form of linear curves specific to PM state at temperatures above the $T_C$.

To determine the magnitude of the MCE, the $\Delta S_M$ values of the samples from the isothermal magnetization curves are calculated using the approximated Maxwell's thermodynamic relation [40]:

$$|\Delta S_M| = \sum_i \frac{M_i - M_{i+1}}{T_{i+1} - T_i} \Delta H, \quad (1)$$

where $M_i$ and $M_{i+1}$ are the magnetizations at $T_i$ and $T_{i+1}$, respectively. The temperature dependent $\Delta S_M$ curves obtained at different magnetic fields are given in Fig. 7. Since the $\Delta S_M$ is a magnitude proportional to change of magnetization, it goes to a maximum in the $T_C$ region where the greatest change occurs. From Fig. 7, it is seen that the $\Delta S_M$ curves of the samples go to maximum at their $T_C$ temperatures, supporting this explanation. With the increase in the applied magnetic field value, the $\Delta S_M$ values increased, as expected, depending on the increase in the number of magnetic moments in the direction of the magnetic field. Furthermore, the peak of $\Delta S_M$ curves over a wide temperature range reveals that the magnetic phase transition has a second order character [41]. The maximum magnetic entropy change ($\Delta S_M{}^{max}$) values are determined as in Table 3 at different magnetic fields. These values are larger than the results given in the literature of doping to Mn-site in different manganite materials [34, 42-45]. It is clear from the Table 3 that the $\Delta S_M{}^{max}$ values decreased with the increase of Ni amount as in the $T_C$. This decrement is due to the decrease in the number of conduction electrons, which also causes a decrease in the $T_C$ due to the increase in the number of $Mn^{4+}$ ($t^3{}_{2g}\, e^0{}_g$) ions with addition of Ni to the structure.

Relative Cooling Power (RCP) expresses technological importance of the MCE and refers to the amount of heat transferred from the hot to cold sinks in an ideal refrigerant cycle [46]. The RCP value of a material can be evaluated from the equation below;

$$RCP = -\Delta S_M{}^{max} \times \delta T_{FWHM} \quad (2)$$

where $\delta T_{FWHM}$ shows full width of the $\Delta S_M$ curve at half maximum [46]. RCP values are calculated for all samples and shown in Table 3. Initially, the RCP value increased with the expansion of the temperature range of the $\Delta S_M$ curve with the addition of Ni to the structure, but it systematically decreased with the increase of the Ni concentration.

For the purpose of understanding the nature of the transition from FM to PM state, curves of $H/M$ vs. $M^2$, called as Arrott plots, are evaluated from these $M(H)$ curves. Figure 8

shows the Arrott plots for all samples. The Banerjee criterion [47] states that the magnetic phase transition has a second-order transition if the Arrott curves around the $T_C$ have a positive slope and a first-order transition otherwise. From the Fig. 8, it can be said that the samples have a second-order transition due to their positive slope in $T_C$ region. Materials showing second-order magnetic phase transition are more advantageous than those with first-order transition because they have low thermal and magnetic hysteresis, which is of great importance for technological requirements [48]. It is seen from the Arrott curves of each sample at its transition temperature that the curves pass through the origin. This signifies that there is a true long range FM interaction [42]. Another method that verifies the second-order phase transition is the universal master curve proposed by Franco [49]. In this method, $\Delta S_M$ values are normalized to its maximum value and the temperature axis is rescaled according to the equations below [49];

$$\theta = \begin{cases} -(T - T_C)/(T_{r1} - T_C) & T \leq T_C \\ (T - T_C)/(T_{r2} - T_C) & T > T_C \end{cases} \quad (3)$$

where $T_{r1}$ and $T_{r2}$ are the temperatures below and above $T_{peak}$. These temperatures are values corresponding to the arbitrary value of $h$<1 to $\Delta S_M(T_{r1,2}) / \Delta S_M{}^{peak} = h$. Figure 9 shows the normalized $\Delta S_M$ vs. $\theta$ at different applied fields. It is clear from the figure that the normalized entropy change curves overlap on a single curve for all samples. This shows that the magnetic phase transition is second-order.

To identify the magnetic phase transition's order, the Landau theory which takes into account the electron interaction and magneto-elastic coupling effects is also used [50]. For a sample exhibiting second-order phase transition at temperatures near $T_C$, the Gibbs free energy depended on magnetization and temperature can be written as the following equation.

$$G(M,T) = \frac{a(T)}{2}M^2 + \frac{b(T)}{4}M^4 + \frac{c(T)}{6}M^6 + \ldots\ldots - \mu_0 H. \quad (4)$$

In Eq. (4), the terms of a, b, c are known as Landau coefficients. The temperature dependence of Landau coefficients has been calculated for all samples, and the ones for LSM and LSM6 manganite are given in Figs. 10 (a-b). Information about the type of the magnetic phase transition can be provided from the Landau theory. [19, 51]. The *a* coefficient gets a minimum value at temperatures near $T_C$. The *b* coefficient including the elastic and the magnetoelastic terms of free energy determines the type of magnetic phase transition [52]. If the *b* coefficient is positive at $T_C$, it is second order [53]. Around $T_C$, the value of the *b* coefficient is positive for the samples as seen from Figs. 10 (a-b). This expresses that the phase

transition for the samples is second order. The *c* coefficient affected by experimental errors is a constant. This coefficient is always positive at $T_C$ [54].

According to the energy minimization, for a magnetic system; the equation of state system can be given as:

$$\frac{H}{M} = a(T) + b(T)M^2 + c(T)M^4 \quad (5)$$

The theoretical $-\Delta S_M$ value of the FM materials is computed by;

$$-\Delta S_M = \left(\frac{\partial G}{\partial T}\right)_H = \frac{1}{2}a'(T)M^2 + \frac{1}{4}b'(T)M^4 + \frac{1}{6}c'(T)M^6 \quad (6)$$

Figure 10 (c) shows the temperature dependence of the theoretical and experimental $-\Delta S_M$ curves for 5T. The obtained $-\Delta S_M$ are in agreement with each other above $T_C$ temperatures. This result gives information that the magnetoelastic coupling and electron interactions may alter both $-\Delta S_M$ values and the temperature dependence of the $-\Delta S_M$ curves [55-56]. Below $T_C$ temperatures, there are differences between the obtained experimental values. This may arise from the Jahn–Teller effect, exchange interactions and micromagnetism [57].

## 4. Conclusions

The effect of Ni substitution with Mn in $La_{0.7}Sr_{0.3}MnO_3$ manganite on structural, magnetic and MC properties was studied. Sol-gel technique was used in synthesis samples. It has been observed from XRD spectra that the samples have mono-phase and rhombohedral symmetry. *M(T)* showed that the samples change from the FM to the PM state with increasing the temperature. $T_C$ temperatures are determined as 363, 351, 344 and 324 K for LSM, LSM2, LSM4 and LSM6, respectively. The $T_C$ decreased with the increase of the Ni concentration. This situation is attributed to the fact that the DE interaction is weakened due to the increase in the $Mn^{4+}$ number in the structure with the increase of Ni concentration. $\Delta S_M$ of the samples were determined from the *M(H)* measurements taken in the regions of $T_C$. $\Delta S_M{}^{max}$ values were calculated as 4.52, 4.51, 4.41 and 3.90 $Jkg^{-1}K^{-1}$ for LSM, LSM2, LSM4 and LSM6 at 5T, respectively. The magnetic phase transitions were determined as second-order from the Arrott curves and universal master curves for the samples. Results showed that the technologically important RCP values increased with the expansion of the temperature range of the $\Delta S_M$ curve with the addition of Ni to the structure. These results are important in terms of bringing the $T_C$

of the $La_{0.7}Sr_{0.3}MnO_3$ manganite to room temperature without causing too much decrease in $\Delta S_M$ values and with the improvement in RCP values.

**Acknowledgements**

This work is supported by the TUBITAK (The Scientific and Technological Research Council of Turkey) under grant contract no. 119F069.

**References**

[1] B. Dorin, J. Avsec, A. Plesca, 2018. "The Efficiency of Magnetic Refrigeration and a Comparison with Compressor Refrigeration Systems", Journal of Energy Technology 11(2018) 59-69.

[2] M.H. Phan, S. C. Yu, "Review of the magnetocaloric effect in manganite materials", Journal of Magnetism and Magnetic Materials 308 (2007) 325-340.

[3] T. Gottschall, K. P. Skokov, M. Fries, A. Taubel, I. Radulov, F. Scheibel, D. Benke, S. Riegg, O. Gutfleisch, "Making a Cool Choice: The Materials Library of Magnetic Refrigeration", Adv. Energy Mater. 9, (2019) 1901322 (1-13).

[4] A. Kitanovski, "Energy Applications of Magnetocaloric Materials", Adv. Energy Mater. 10 (2020) 1903741 (1-34).

[5] A. M. Tishin, Y. I. Spichkin, V. I. Zverev, P.W. Egolf, "A review and new perspectives for the magnetocaloric effect: New materials and local heating and cooling inside the human body", International Journal of Refrigeration 68 (2016) 177-186.

[6] Tishin, A. M., Spichkin, Y.I., 2003. The magnetocaloric effect and its Applications, IOP Publishing LTD.

[7] M. Khlifi, M. Bejar, O. EL Sadek, E. Dhahri, M. A. Ahmed, E. K. Hlil, "Structural, magnetic and magnetocaloric properties of the lanthanum deficient in $La_{0.8}Ca_{0.2-x}MnO_3$ (x = 0–0.20) manganites oxides", Journal of Alloys and Compounds (2011) 7410–7415.

[8] K. A. Gschneidner, V. K. Pecharsky, A. O. Tsokol, "Recent developments in magnetocaloric materials", Rep. Prog. Phys. 68 (2005) 1479–1539.

[9] C. R. H. Bahl, D. Velazquez, K. K. Nielsen, K. Engelbrecht, K.B. Andersen, R. Bulatova, N. Pryds, "High performance magnetocaloric perovskites for magnetic refrigeration", Appl. Phys. Lett. 100 (2012) 121905.

[10] A. M. J. Mahdy, "Overview for published Magnetocaloric Materials used in Magnetic Refrigeration applications", International Journal of Computation and Applied Sciences IJOCAAS, Vol. 3, Issue 1 (2017) ISSN: 2399-4509.

[11] J. Lyubina, "Magnetocaloric materials for energy efficient cooling", J. Phys. D: Appl. Phys. 50 (2017) 053002 (28pp).

[12] O. Sari, M. Balli, "From conventional to magnetic refrigerator technology", International Journal of Refrigeration 37 (2014) 8-15.

[13] E. Brück, O. Tegus, D. T. C. Than, N. T. Trung, K. H. J. Buschow, "A review on Mn based materials for magnetic refrigeration: Structure and properties", International Journal of Refrigeration 31 (2008) 763–770.

[14] A. Barman, S. Kar-Narayan, D. Mukherjee, "Caloric Effects in Perovskite Oxides", Adv. Mater. Interfaces (2019) 1900291.

[15] N. Chau, H. N. Nhat, N. H. Luong, D. L. Minh, N. D. Tho, N. N. Chau, "Structure, magnetic, magnetocaloric and magnetoresistance properties of $La_{1-x}Pb_xMnO_3$ perovskite," Phys. B 327 (2003) 270–278.

[16] M. S. Reis, V. S. Amaral, J. P. Araujo, P. B Tavares, A. M. Gomes, I. S. Oliveira, "Magnetic entropy change of $Pr_{1-x}Ca_xMnO_3$ manganites ($0.2 \leqslant x \leqslant 0.95$)", Phys. Rev. B. 71 (2005) 144413–144418.

[17] W. Zhong, W. Chen, C. T. Au, Y. W. Du, "Dependence of the magnetocaloric effect on oxygen stoichiometry in polycrystalline $La_{2/3}Ba_{1/3}MnO_{3-\delta}$", J. Magn. Magn. Mater. 261 (2003) 238–243.

[18] G. F. Wang, L. R. Li, Z. R. Zhao, X. Q. Yu, X. F. Zhang, "Structural and magnetocaloric effect of $Ln_{0.67}Sr_{0.33}MnO_3$ (Ln=La, Pr and Nd) nanoparticles", Ceram. Int. 40 (2014)16449–16454.

[19] G. Akça, S. Kılıç Çetin, A. Ekicibil, "Structural, magnetic and magnetocaloric properties of $(La_{1-x}Sm_x)_{0.85}K_{0.15}MnO_3$ (x = 0.0, 0.1, 0.2 and 0.3) perovskite manganites", Ceram. Int. 43 (2017) 15811–15820.

[20] A. O. Ayaş, M. Akyol, A. Ekicibil, "Structural and magnetic properties with largereversible magnetocaloric effect in $(La_{1-x}Pr_x)_{0.85}Ag_{0.15}MnO_3$ ($0.0 \leqslant x \leqslant 0.5$) compounds", Philos. Mag. 96 (2016) 922.

[21] O. Hassayoun, M. Baazaoui, M. R. Laouyenne, F. Hosni, E.K. Hlil, M. Oumezzine, Kh. Farah, "Magnetocaloric effect and electron paramagnetic resonance studies of the transition from ferromagnetic to paramagnetic in $La_{0.8}Na_{0.2}Mn_{1-x}Ni_xO_3$ ($0 \leq x \leq 0.06$)", Journal of Physics and Chemistry of Solids 135 (2019) 109058.

[22] M. H. Phan, H. X. Peng, S.C. Yu, N. D. Tho, N. Chau, "Large magnetic entropy change in Cu-doped manganites", Journal of Magnetism and Magnetic Materials 285 (2005) 199–203.

[23] N. Kallel, S. Kallel, A. Hagaza, M. Oumezzine, "Magnetocaloric properties in the Cr-doped $La_{0.7}Sr_{0.3}MnO_3$ manganites", Physica B 404 (2009) 285–288.

[24] N. Chau, P. Q. Niem, H. N. Nhat, N. H. Luong, N. D. Tho, "Influence of Cu substitution for Mn on the structure, magnetic, magnetocaloric and magnetoresistance properties of $La_{0.7}Sr_{0.3}MnO_3$ perovskites", Physica B 327 (2003) 214–217.

[25] A. Selmi, R. M'nassri, W. Cheikhrouhou-Koubaa, N. C. Boudjada, A. Cheikhrouhou, "The effect of Co doping on the magnetic and magnetocaloric properties of $Pr_{0.7}Ca_{0.3}Mn_{1-x}Co_xO_3$ manganites", Ceramics International41 (2015) 7723–7728.

[26] V. Dyakonov, A. Ślawska-Waniewska, N. Nedelko, E. Zubov, V. Mikhaylov, K. Piotrowski, A. Szytuła, S. Baran, W. Bazela, Z. Kravchenko, P. Aleshkevich, A. Pashchenko, K. Dyakonov, V. Varyukhin, H. Szymczak, "Magnetic, resonance and transport properties of nanopowder of $La_{0.7}Sr_{0.3}MnO_3$ manganites", Journal of Magnetism and Magnetic Materials 322 (2010) 3072–3079.

[27] P. T., Phong, N. V. Dang, L. V. Bau, N. M. An, I. Lee, "Landau mean-field analysis and estimation of the spontaneous magnetization from magnetic entropy change in $La_{0.7}Sr_{0.3}MnO_3$ and $La_{0.7}Sr_{0.3}Mn_{0.95}Ti_{0.05}O_3$", Journal of Alloys and Compounds 698 (2017) 451-459.

[28] R. Cherif, S. Zouari, M. Ellouze, E. K. Hlil, F. Elhalouani, "Structural, magnetic and magnetocaloric properties of $La_{0.7}Sr_{0.3}MnO_3$ manganite oxide prepared by the ball milling method", Eur. Phys. J. Plus, (2014) 129: 83.

[29] R. Cherif, E.K. Hlil, M. Ellouze, F. Elhalouani, S. Obbade, Magnetic and magnetocaloric properties of $La_{0.6}Pr_{0.1}Sr_{0.3}Mn_{1-x}Fe_xO_3$ manganites", Journal of Solid State Chemistry 215 (2014) 271–276.

[30] G. Akça, S. Kılıç Çetin, A. Ekicibil, Composite $xLa_{0.7}Ca_{0.2}Sr_{0.1}MnO_3$ /(1−x) $La_{0.7}Te_{0.3}MnO_3$ materials: magnetocaloric properties around room temperature", Journal of Materials Science: Materials in Electronics (2020) 31:6796–6808.

[31] H. Rahmouni, M. Nouiri, R. Jemai, N. Kallel, F. Rzigua, A. Selmi,, K. Khirouni, S. Alaya, "Electrical conductivity and complex impedance analysis of 20% Ti-doped $La_{0.7}Sr_{0.3}MnO_3$ perovskite", Journal of Magnetism and Magnetic Materials 316 (2007) 23–28.

[32] S. Kılıç Çetin, G. Akça, A. Ekicibil, "Impact of small Er rare earth element substitution on magnetocaloric properties of $(La_{0.9}Er_{0.1})_{0.67}Pb_{0.33}MnO_3$ perovskite", Journal of Molecular Structure 1196 (2019) 658-661.

[33] Y. Zhang, "Local structure and magnetocaloric effect for $La_{0.7}Sr_{0.3}Mn_{1-x}Ni_xO_3$", Current Applied Physics (2012), 803-807.

[34] Abd El-Moez A. Mohamed, B. Hernando, A. M. Ahmed, "Magnetic, magnetocaloric and thermoelectric properties of nickel doped manganites", Journal of Alloys and Compounds 692 (2017) 381-387.

[35] R. Mouta, R. X. Silva, C. W. A. Paschoal, "Tolerance factor for pyrochlores and related structures", Acta Cryst. (2013) B69, 439–445.

[36] Z. Wang, Q. Xub, K. Chen, "Maximum magnetic entropy change modulated toward room temperature in perovskite manganites $La_{0.7-x}Nd_x(Ca,Sr)_{0.3}MnO_3$", Curr. Appl. Phys. 12 (2012) 1153–1157.

[37] R. D. Shannon, "Revised effective ionic radii and systematic studies of interatomic distances in halides and chalcogenides", Acta Cryst. (1976). A32, 751-767.

[38] K. Laajimi, M. Khlifi, E. K. Hlil, K. Taibi, M.H. Gazzah, J. Dhahri, "Room Temperature magnetocaloric effect and critical behavior in $La_{0.67}Ca_{0.23}Sr_{0.1}Mn_{0.98}Ni_{0.02}O_3$ oxide", Journal of Materials Science: Materials in Electronics, 13 (2019) 11868-11877.

[39] L. P. Gor'kov, V. Z. Kresin, "Mixed-valence manganites: fundamentals and main properties", Physics Reports 400 (2004) 149-208.

[40] V.K. Pecharsky, K.A. Gschneidner Jr., "Magnetocaloric effect from indirect measurements: Magnetization and heat capacity", J. Appl. Phys. 86 (1999) 565-575.

[41] N. Dhahri, A. Dhahri, K. Cherif, J. Dhahr, H. Belmabrouk, E. Dhahri, "Effect of Co substitution on magnetocaloric effect in $La_{0.67}Pb_{0.33}Mn_{1-x}Co_xO_3$ $(0.15\leq x\leq 0.3)$", Journal of Alloys and Compounds 507 (2010) 405–409.

[42] A. Selmi, R. M'nassri, W. Cheikhrouhou-Koubaa, N. Chniba Boudjada, A. Cheikhrouhou, "Effects of partial Mn-substitution on magnetic and magnetocaloric properties in $Pr_{0.7}Ca_{0.3}Mn_{0.95}X_{0.05}O_3$ (Cr, Ni, Co and Fe) manganites", Journal of Alloys and Compounds 619 (2015) 627–633.

[43] P. Nisha, S. Savitha Pillai, Azad Darbandi, M.R. Varma, K.G. Sureshand Horst Hahn, "Critical behaviour and magnetocaloric effect of nano crystalline $La_{0.67}Ca_{0.33}Mn_{1-x}Fe_xO_3$ (x = 0.05, 0.2) synthesized by nebulized spray pyrolysis", Mater. Chem. Phys. 136 (2012) 66–74

[44] Pengyue Zhang, Hangfu Yang, Suyin Zhang, Hongliang Ge, Sihao Hua, "Magnetic and magnetocaloric properties of perovskite $La_{0.7}Sr_{0.3}Mn_{1-x}Co_xO_3$", Physica B 410 (2013) 1–4

[45] E. Oumezzine, S. Hcini, E.K. Hlil, E. Dhahri, M. Oumezzine, "Effect of Ni-doping on structural, magnetic and magnetocaloric properties of $La_{0.6}Pr_{0.1}Ba_{0.3}Mn_{1-x}Ni_xO_3$ nanocrystalline manganites synthesized by Pechini sol-gel method", J. Alloys Comp. 615 (2014) 553-560.

[46] V.K. Pecharsky, K.A. Gschneidner, "Magnetocaloric Materials", Annu. Rev. Mater. Sci. 30 (2000) 387-429.

[47] B.K. Banerjee, "On a generalised approach to first and second order magnetic transitions", Phys. Lett. 12 (1964) 16-17.

[48] A. O. Ayaş, "Structural and magnetic properties with reversible magnetocaloric effect in $PrSr_{1-x}Pb_xMn_2O_6$ ($0.1 \leq x \leq 0.3$) double perovskite manganite structures", Philosophical Magazine, 98:30 (2018) 2782-2796.

[49] C.M. Bonilla, J. Herrero-Albillos, F. Bartolome, L.M. Garcia, M. Parra-Borderias, V. Franco, "Universal behavior for magnetic entropy change in magnetocaloric materials: An analysis on the nature of phase transitions", Phys. Rev. B 81 (2010) 224424.

[50] J.S. Amaral, M.S. Reis, V.S. Amaral, T.M. Mendonc¸a, J.P. Araújo, M.A. Sá, P.B. Tavares, J.M. Vieira, " Magnetocaloric effect in Er- and Eu-substituted ferromagnetic La-Sr manganites", J. Magn. Magn. Mater. 290 (2005) 686-689].

[51] A. Krichene, W. Boujelben, "Enhancement of the magnetocaloric effect in composites based on $La_{0.4}Re_{0.1}Ca_{0.5}MnO_3$ (Re= Dy, Gd, and Eu) polycrystalline manganites", Journal of Superconductivity and Novel Magnetism (2018) 31:577-582

[52] J. Fan, L. Pi, L. Zhang, W. Tong, L. Ling, B. Hong, Y. Shi, W.Zhang, D. Lu, Y. Zhang "Magnetic and magnetocaloric properties of perovskite manganite $Pr_{0.55}Sr_{0.45}MnO_3$", Physica B 406 (2011) 2289–2292.

[53] R. Guetari, T. Bartoli , C. B. Cizmas , N. Mliki, L. Bessais, "Structure, magnetic and magnetocaloric properties of new nanocrystalline (Pr, Dy)$Fe_9$ compounds", Journal of Alloys and Compounds 684 (2016) 291-298.

[54] A. Fujita, K. Fukamichi, "Large magnetocaloric effects and landau coefficients of itinerant electron metamagnetic $La(Fe_xSi_{1-x})13$ compounds", IEEE Trans. Magn. 41 (2005) 3490–3492

[55] M. Koubaa, Y. Regaieg, W.C. Koubaa, A. Cheikhrouhou, S. Ammar-Merah, F. Herbst, "Magnetic and magnetocaloric properties of lanthanum manganites with monovalent

elements doping at A-site", Journal of Magnetism and Magnetic Material 323 (2011) 252–257

[56] R. Cherif, E.K. Hlil, M. Ellouze, F. Elhalouani, S. Obbade, "Study of magnetic and magnetocaloric properties of $La_{0.6}Pr_{0.1}Ba_{0.3}MnO_3$ and $La_{0.6}Pr_{0.1}Ba_{0.3}Mn_{0.9}Fe_{0.1}O_3$ perovskite-type manganese oxides", Journal of Material Science 49 (2014) 8244–8251

[57] H. Yang, P. Zhang, Q. Wu, H. Ge, M. Pan, "Effect of monovalent metal substitution on the magnetocaloric effect of perovskite manganites $Pr_{0.5}Sr_{0.3}M_{0.2}MnO_3$ (M=Na, Li, K and Ag)", Journal of Magnetism and Magnetic Materials 324 (2012) 3727–3730

**Table 1.** The lattice parameters, unit cell volume, A-site and Mn-site radius, tolerance factor *t* and grain sizes of $La_{0.7}Sr_{0.3}Mn_{1-x}Ni_xO_3$ samples.

| x | *a* (Å) | *b* (Å) | *c* (Å) | *V* (Å$^3$) | $\langle r_A \rangle$ (Å) | $\langle r_{Mn} \rangle$ (Å) | *t* | Grain Size (μm) |
|---|---|---|---|---|---|---|---|---|
| **0.00** | 5.5006 | 5.5006 | 13.3531 | 349.8966 | 1.384 | 0.6105 | 0.9792 | 0.361 |
| **0.02** | 5.5045 | 5.5045 | 13.3563 | 350.4693 | 1.384 | 0.6095 | 0.9798 | 0.492 |
| **0.04** | 5.5014 | 5.5014 | 13.3501 | 349.9143 | 1.384 | 0.6084 | 0.9802 | 0.414 |
| **0.06** | 5.5015 | 5.5015 | 13.3395 | 349.6491 | 1.384 | 0.6063 | 0.9812 | 0.407 |

**Table 2.** The atomic percentage of the $La_{0.7}Sr_{0.3}Mn_{1-x}Ni_xO_3$ samples.

| x | Atomic Percentage | | | | |
|---|---|---|---|---|---|
| | **La** | **Sr** | **Mn** | **Ni** | **O** |
| 0.00 | 14.37 | 5.48 | 20.26 | 0 | 59.89 |
| 0.02 | 14.72 | 5.41 | 20.76 | 0.48 | 58.63 |
| 0.04 | 14.75 | 5.28 | 20.14 | 0.82 | 59.00 |
| 0.06 | 14.62 | 5.51 | 19.70 | 1.33 | 58.84 |

**Table 3.** Curie temperature, $T_C$, relative cooling power, RCP and maximum magnetic entropy change, $-\Delta S_M^{max}$ for $La_{0.7}Sr_{0.3}Mn_{1-x}Ni_xO_3$ samples.

| x | $T_C$ (K) | RCP (J.kg$^{-1}$) (5T) | $-\Delta S_M^{max}$ (Jkg$^{-1}$K$^{-1}$) | | | | |
|---|---|---|---|---|---|---|---|
| | | | **1 T** | **2 T** | **3 T** | **4 T** | **5 T** |
| 0.00 | 363 | 219 | 1.57 | 2.51 | 3.26 | 4.09 | 4.52 |
| 0.02 | 351 | 235 | 1.47 | 2.46 | 3.25 | 3.92 | 4.51 |
| 0.04 | 344 | 233 | 1.40 | 2.35 | 3.11 | 3.79 | 4.41 |
| 0.06 | 324 | 200 | 1.17 | 2.21 | 2.84 | 3.55 | 3.90 |

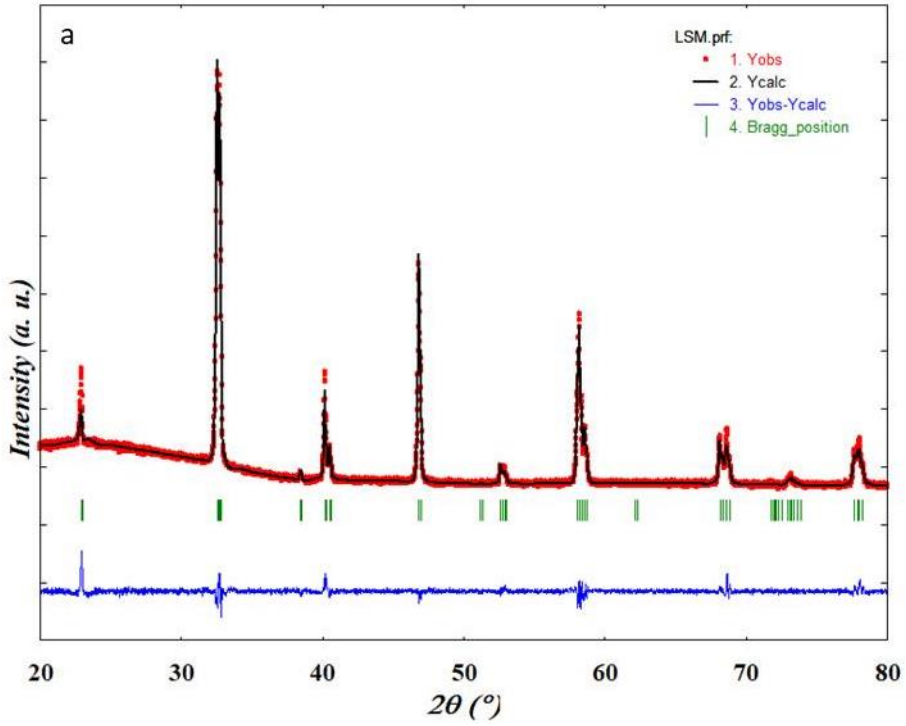
a
LSM.prf:
1. Yobs
2. Ycalc
3. Yobs-Ycalc
4. Bragg_position
Intensity (a. u.)
20
30
40
50
60
70
80
2θ (°)

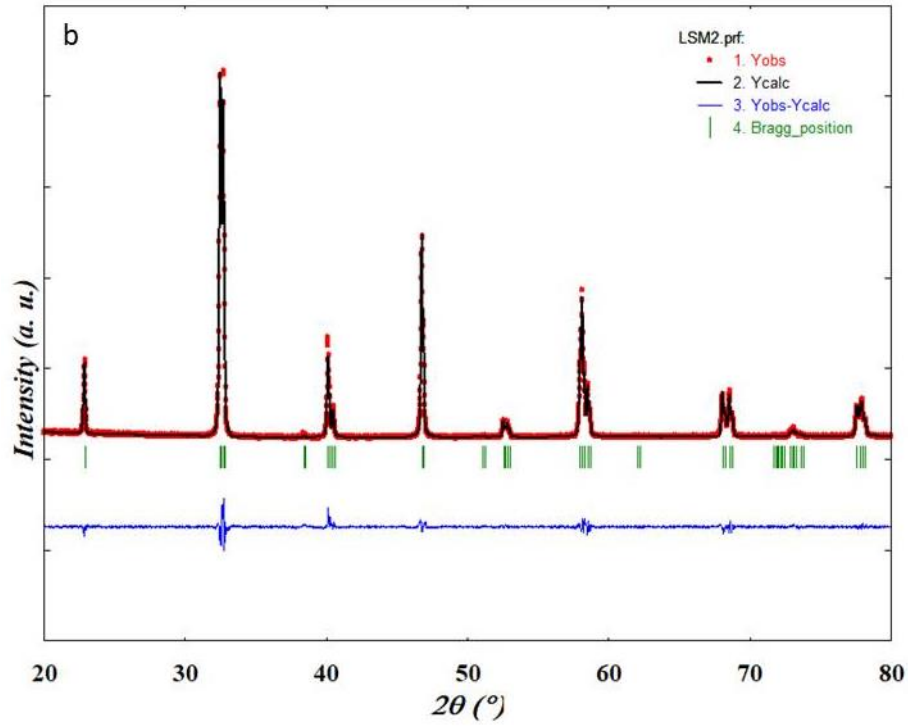
b
LSM2.prf:
1. Yobs
2. Ycalc
3. Yobs-Ycalc
4. Bragg_position
Intensity (a. u.)
20
30
40
50
60
70
80
2θ (°)

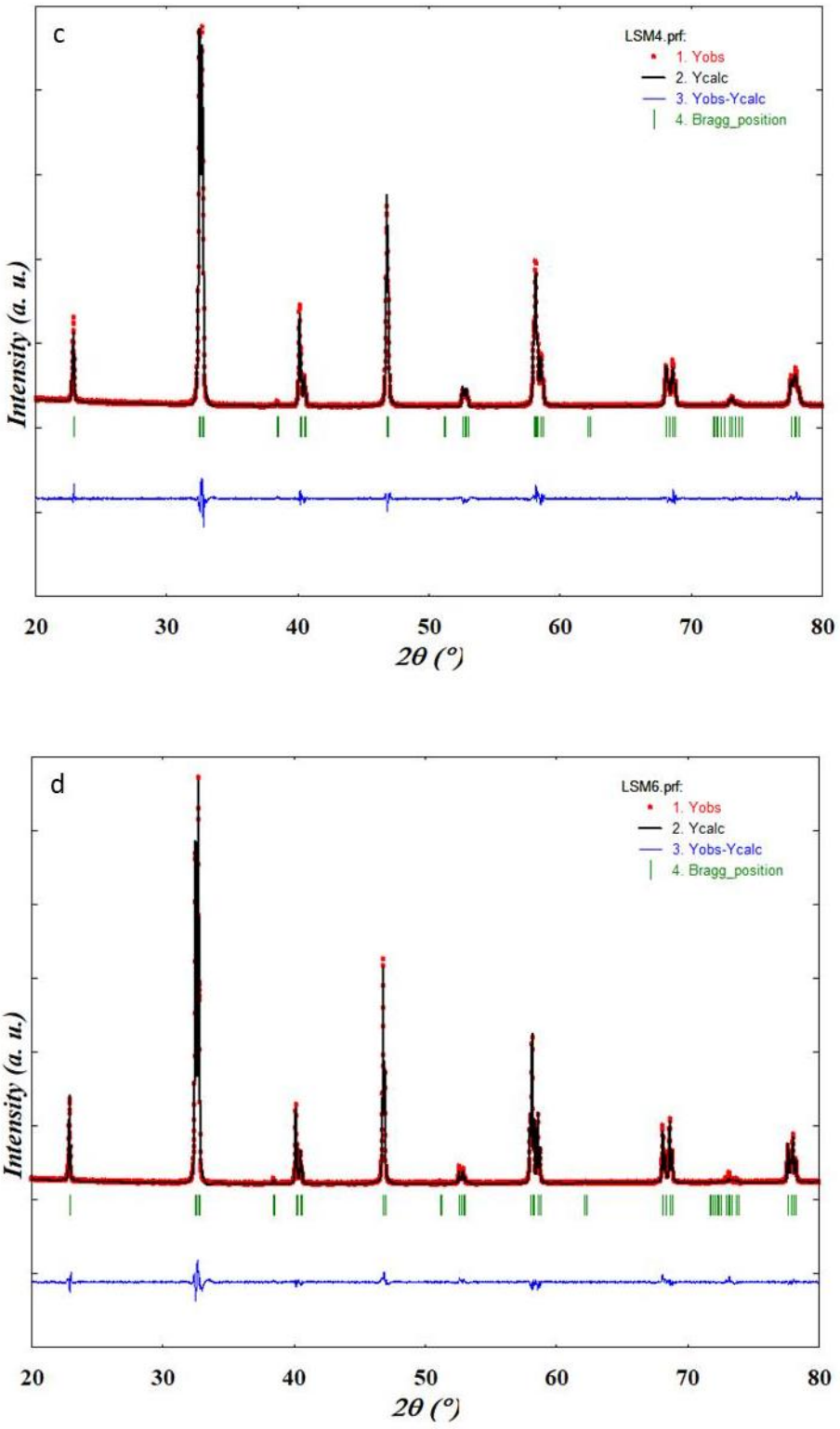


Figure 1. The XRD pattern of $La_{0.7}Sr_{0.3}Mn_{1-x}Ni_xO_3$ (x = 0.00, 0.02, 0.04, 0.06) samples. The observed and calculated data are solid circle (red) and solid line (black) respectively. The blue line is the difference between the observed and calculated data. The positions of Bragg position reflection are represented by vertical green ticks.

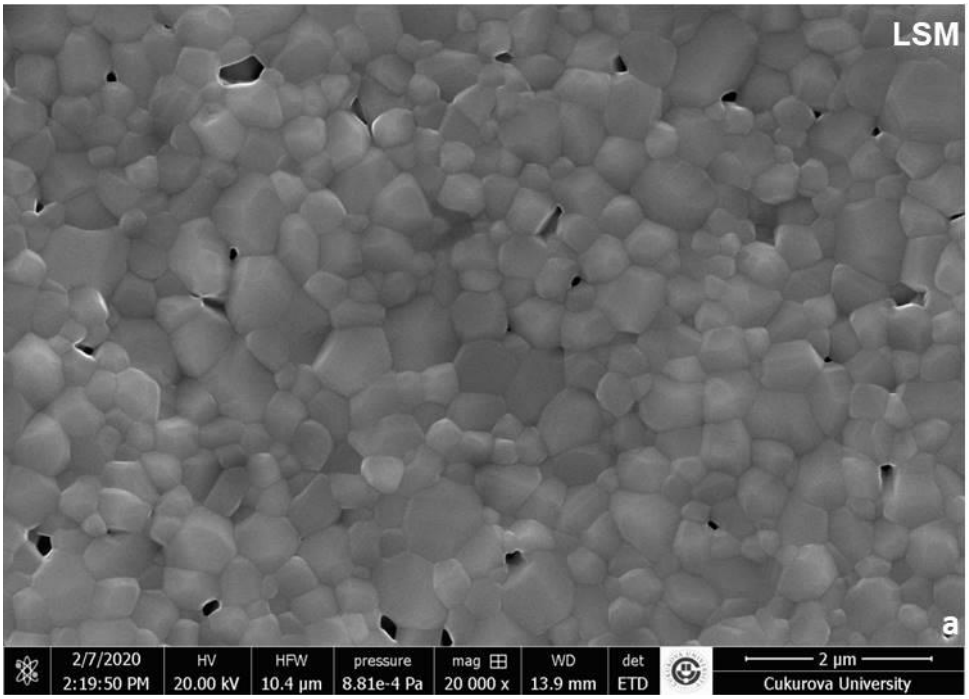
LSM
a
2/7/2020
2:19:50 PM
HV
20.00 kV
HFW
10.4 µm
pressure
8.81e-4 Pa
mag
20 000 x
WD
13.9 mm
det
ETD
2 µm
Cukurova University

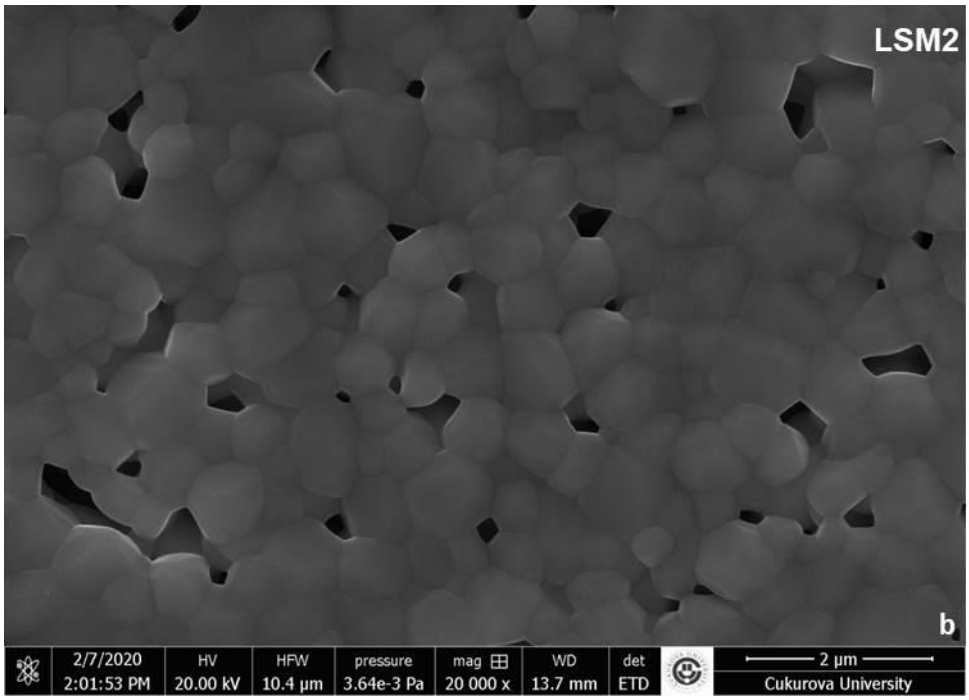
LSM2
b
2/7/2020
2:01:53 PM
HV
20.00 kV
HFW
10.4 µm
pressure
3.64e-3 Pa
mag
20 000 x
WD
13.7 mm
det
ETD
2 µm
Cukurova University

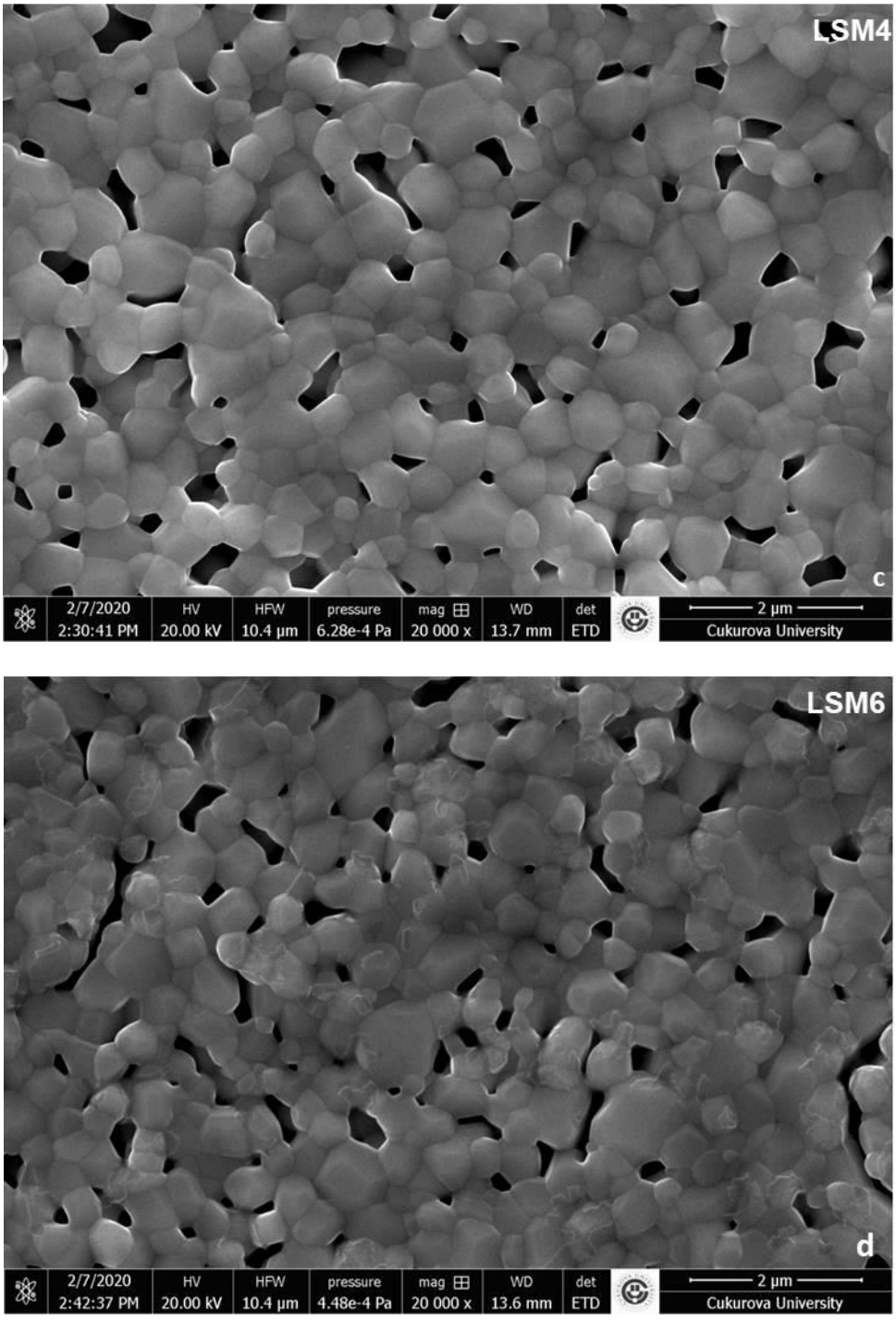


Figure 2. SEM images of $La_{0.7}Sr_{0.3}Mn_{1-x}Ni_xO_3$ (x = 0.00, 0.02, 0.04, 0.06) samples taken at 20 KX magnifications.

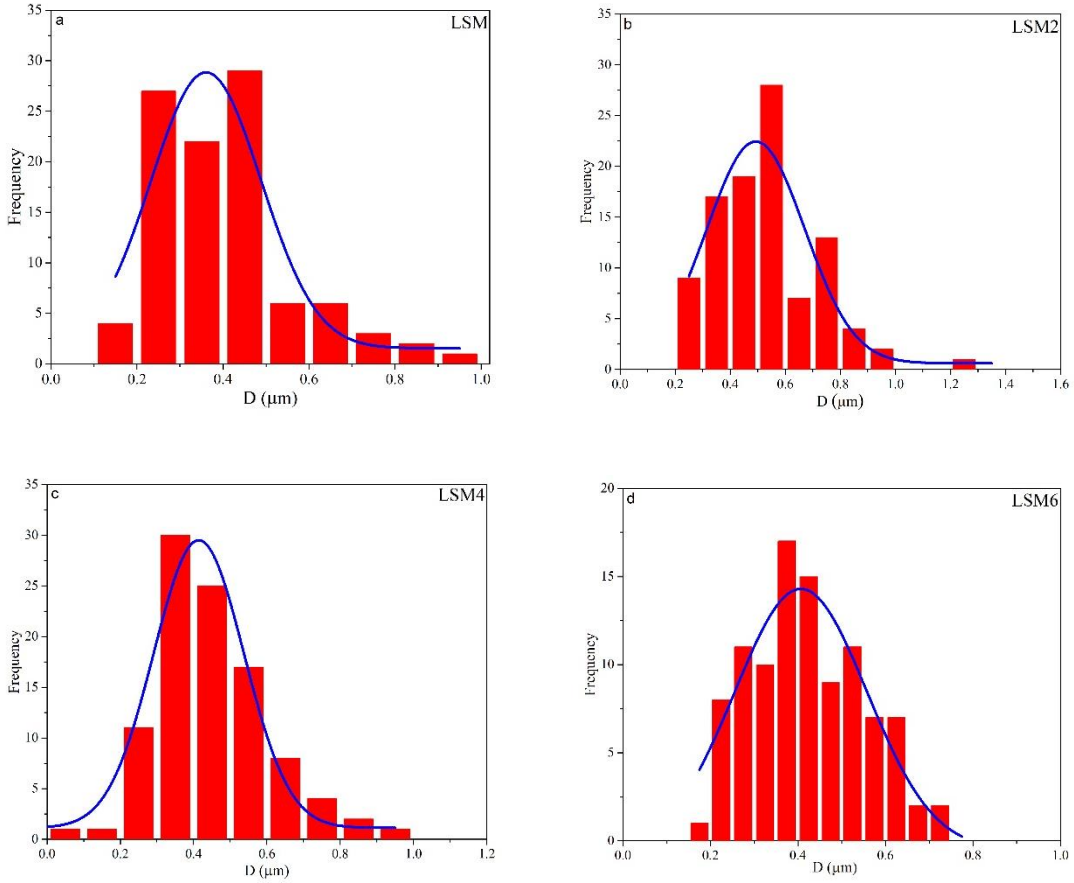


Figure 3. The size distribution histogram of $La_{0.7}Sr_{0.3}Mn_{1-x}Ni_xO_3$ (x = 0.00, 0.02, 0.04, 0.06) samples.

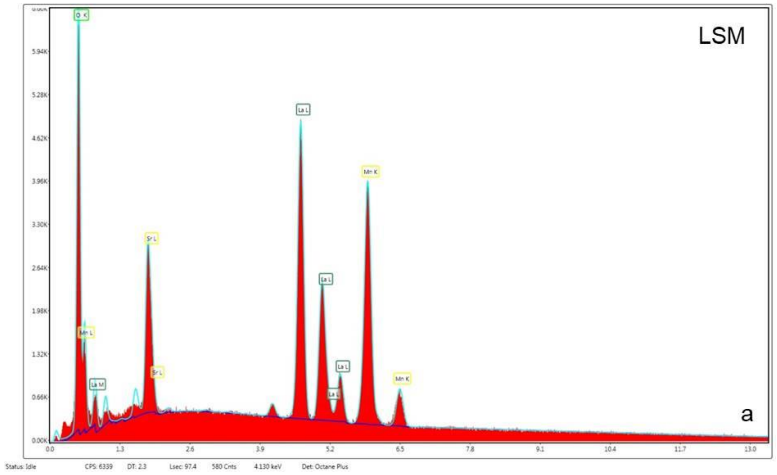

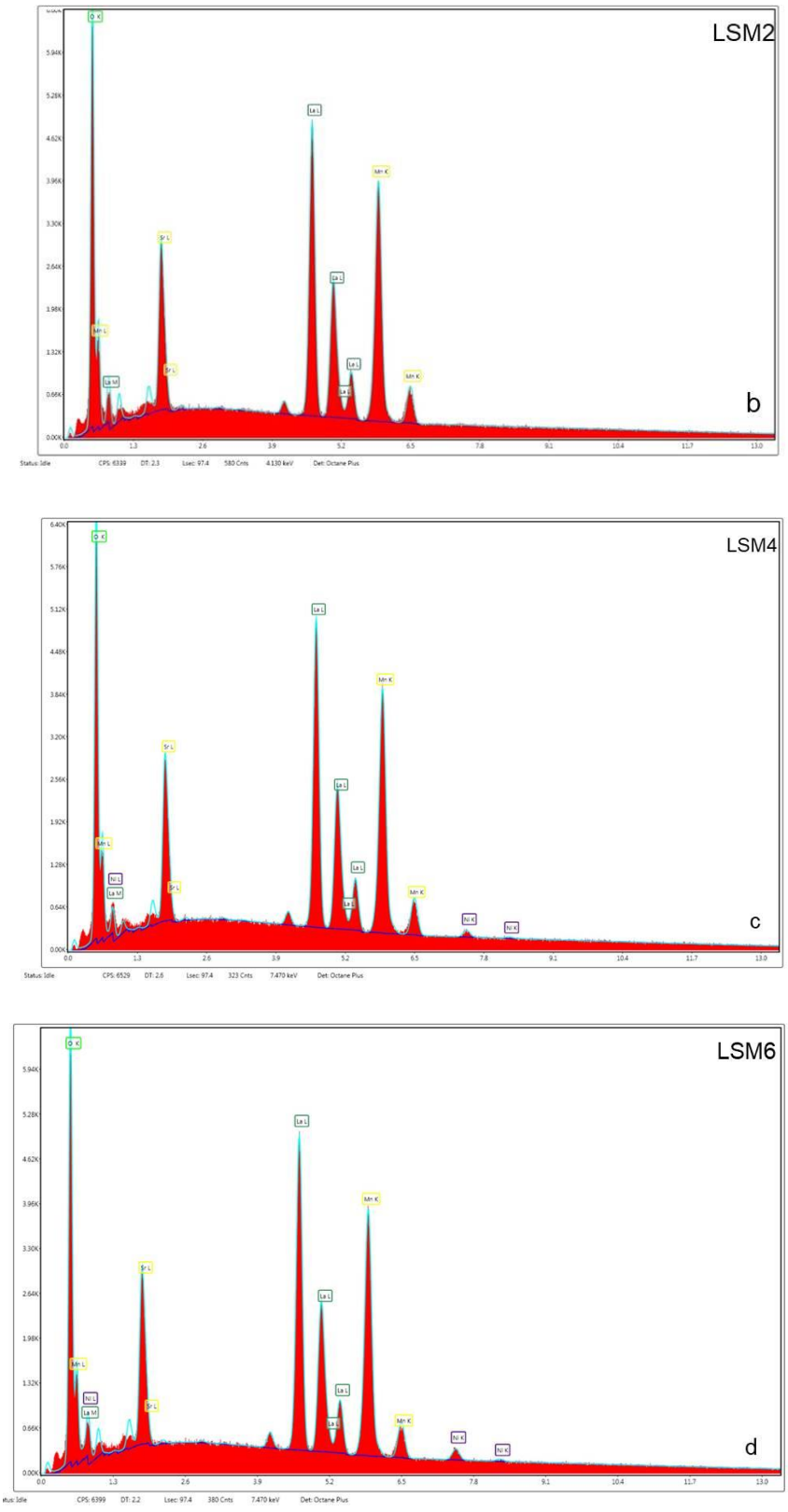


Figure 4. EDS spectra of $La_{0.7}Sr_{0.3}Mn_{1-x}Ni_xO_3$ (x = 0.00, 0.02, 0.04, 0.06) samples.

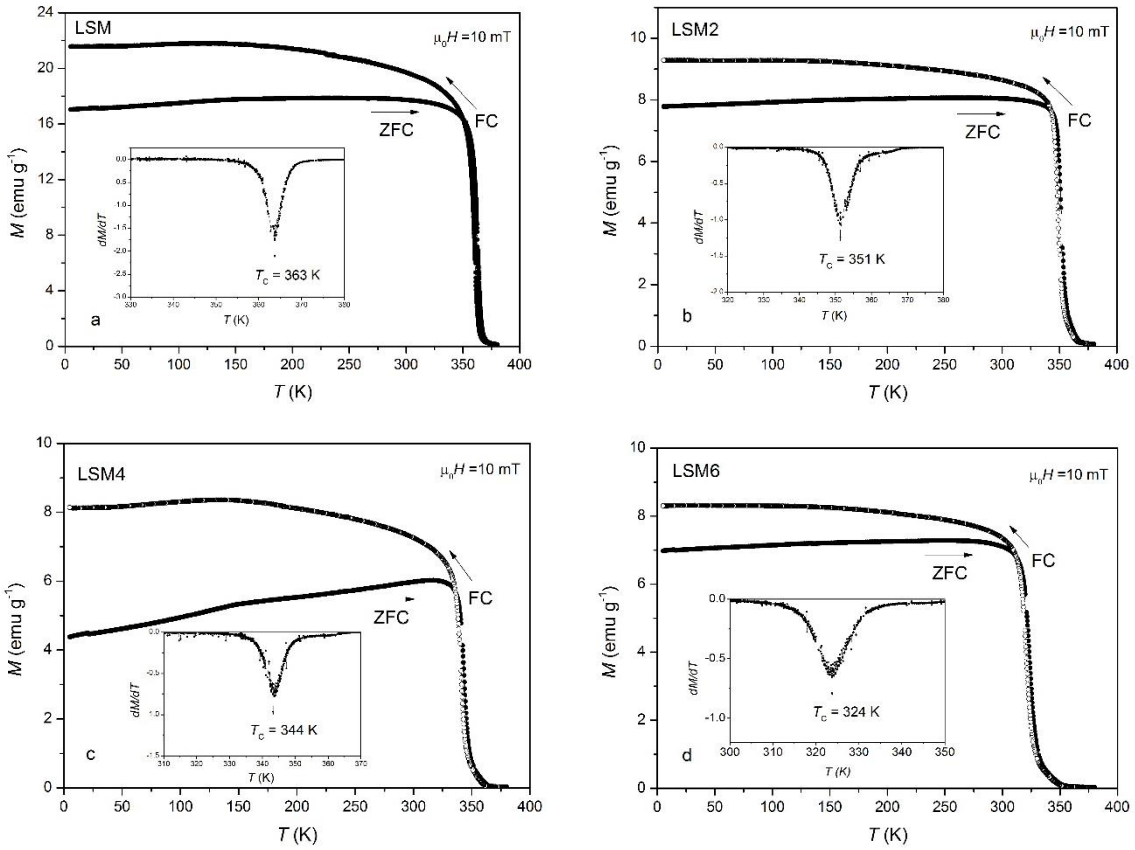


Figure 5. $M(T)$ curves of $La_{0.7}Sr_{0.3}Mn_{1-x}Ni_xO_3$ (x = 0.00, 0.02, 0.04, 0.06) samples. Insets: Temperature dependence of dM/dT.

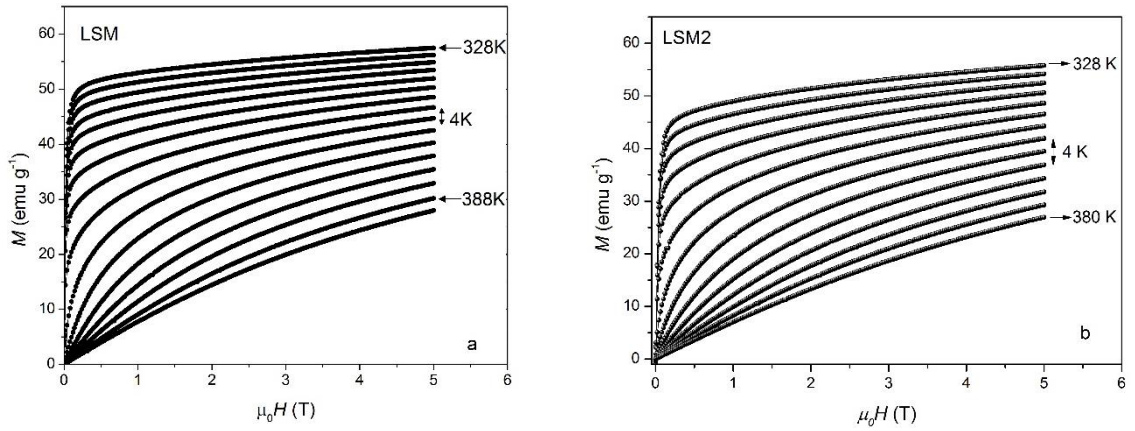

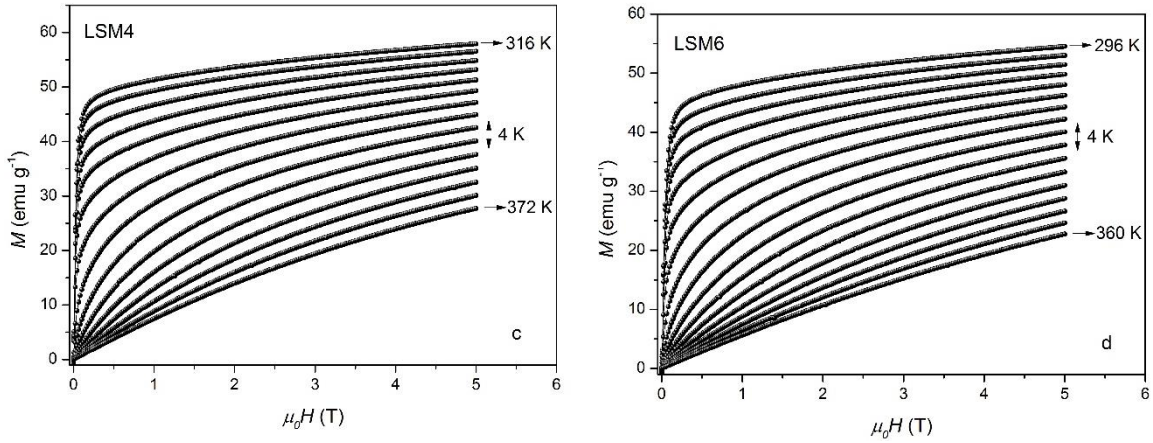


Figure 6. $M(H)$ curves of $La_{0.7}Sr_{0.3}Mn_{1-x}Ni_xO_3$ (x = 0.00, 0.02, 0.04, 0.06) samples.

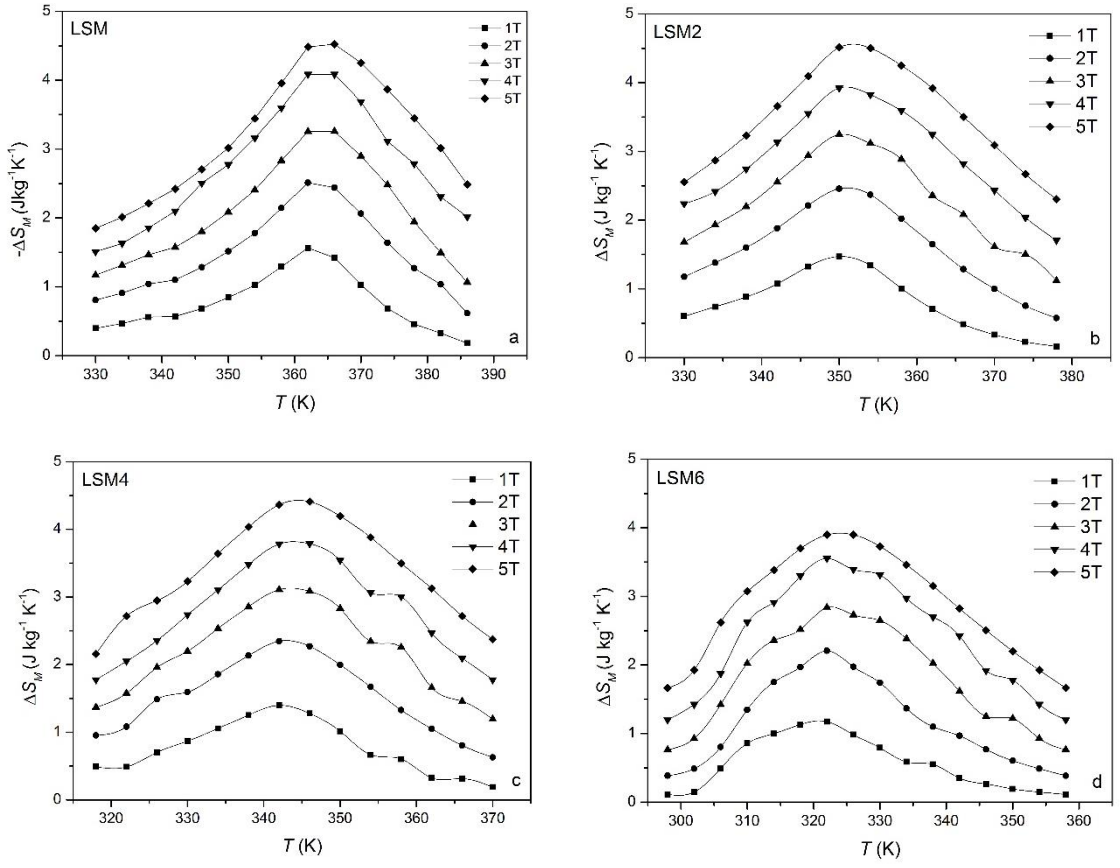


Figure 7. $\Delta S_M(T)$ curves of $La_{0.7}Sr_{0.3}Mn_{1-x}Ni_xO_3$ (x = 0.00, 0.02, 0.04, 0.06) samples at different applied magnetic fields.

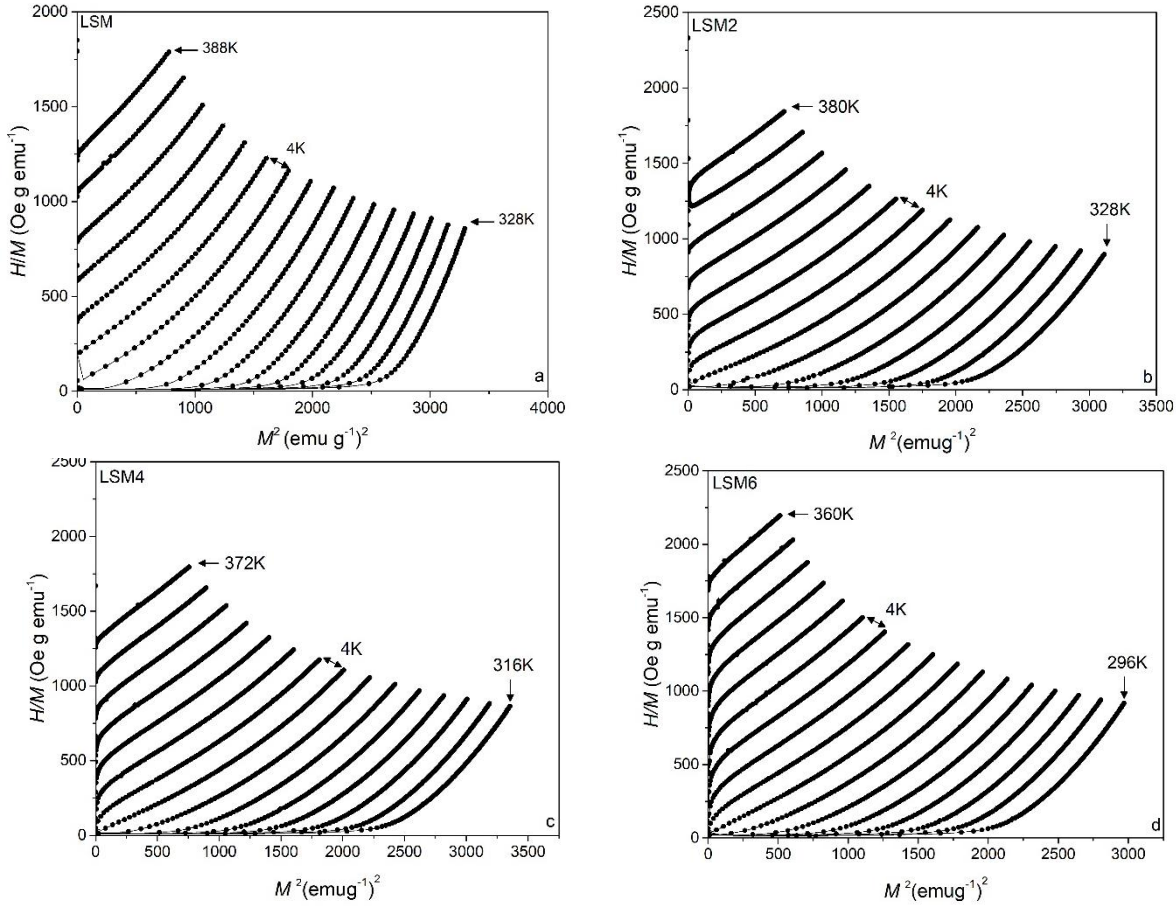


Figure 8. Arrott plots of $La_{0.7}Sr_{0.3}Mn_{1-x}Ni_xO_3$ (x = 0.00, 0.02, 0.04, 0.06) samples.

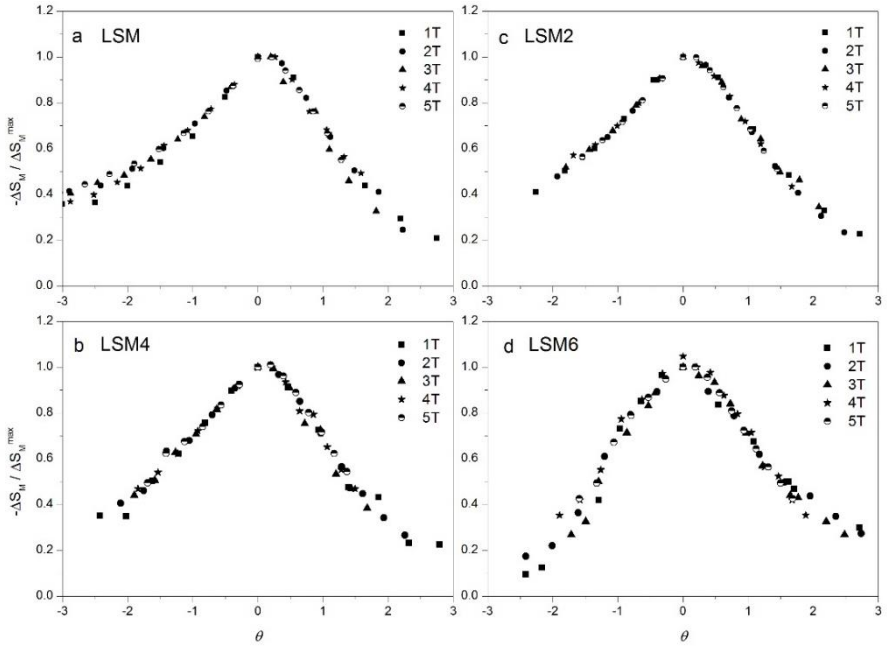


Figure 9. Rescaled temperature $\theta$ versus normalized magnetic entropy change curves at different magnetic field for $La_{0.7}Sr_{0.3}Mn_{1-x}Ni_xO_3$ (x = 0.00, 0.02, 0.04, 0.06) samples.

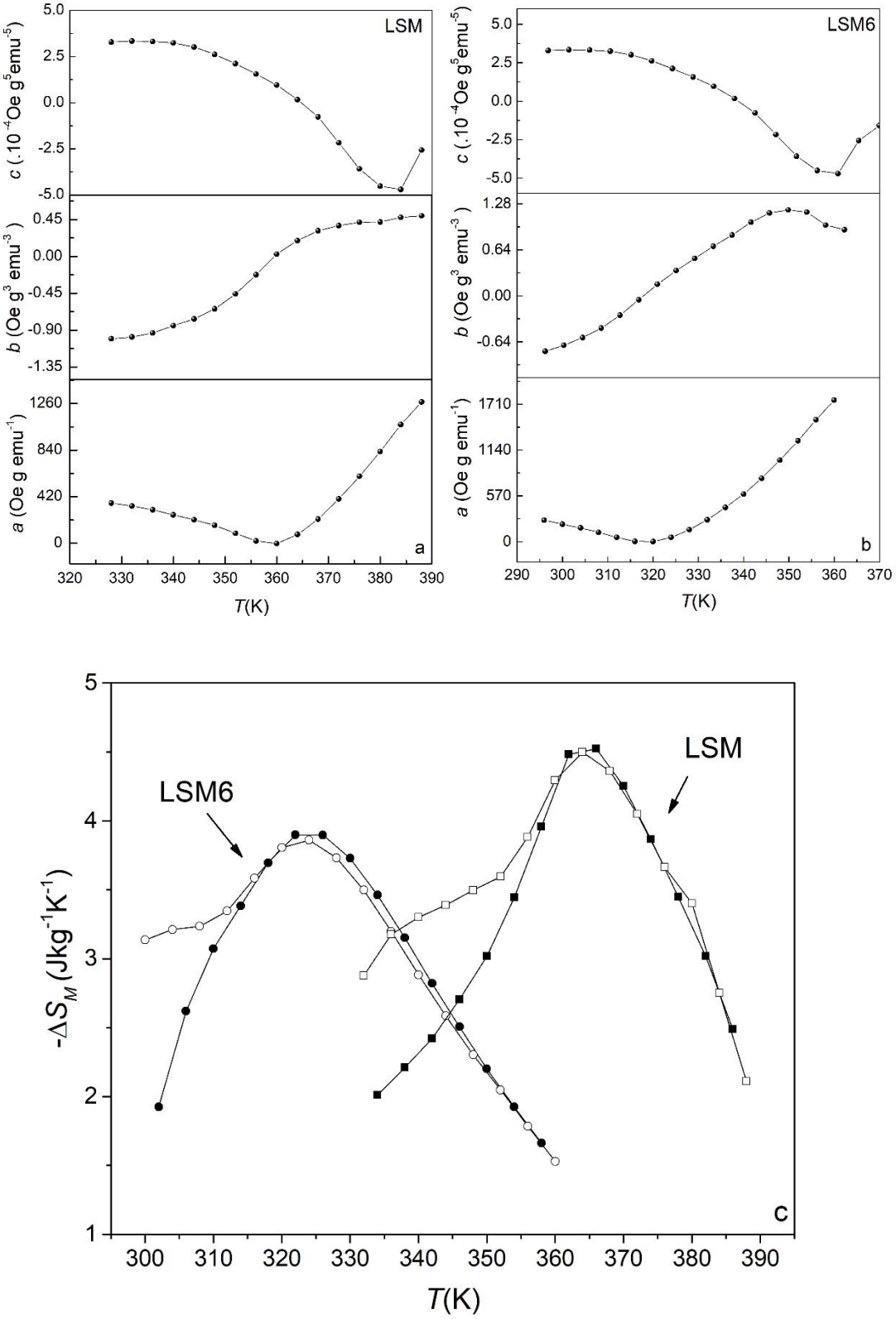


Figure 10. The temperature dependence of the Landau coefficients for (a) LSM and (b) LSM6. The temperature dependence of the experimental and theoretical $-\Delta S_M$ curves for LSM and LSM6 samples under magnetic field of 5 T.

# Figures

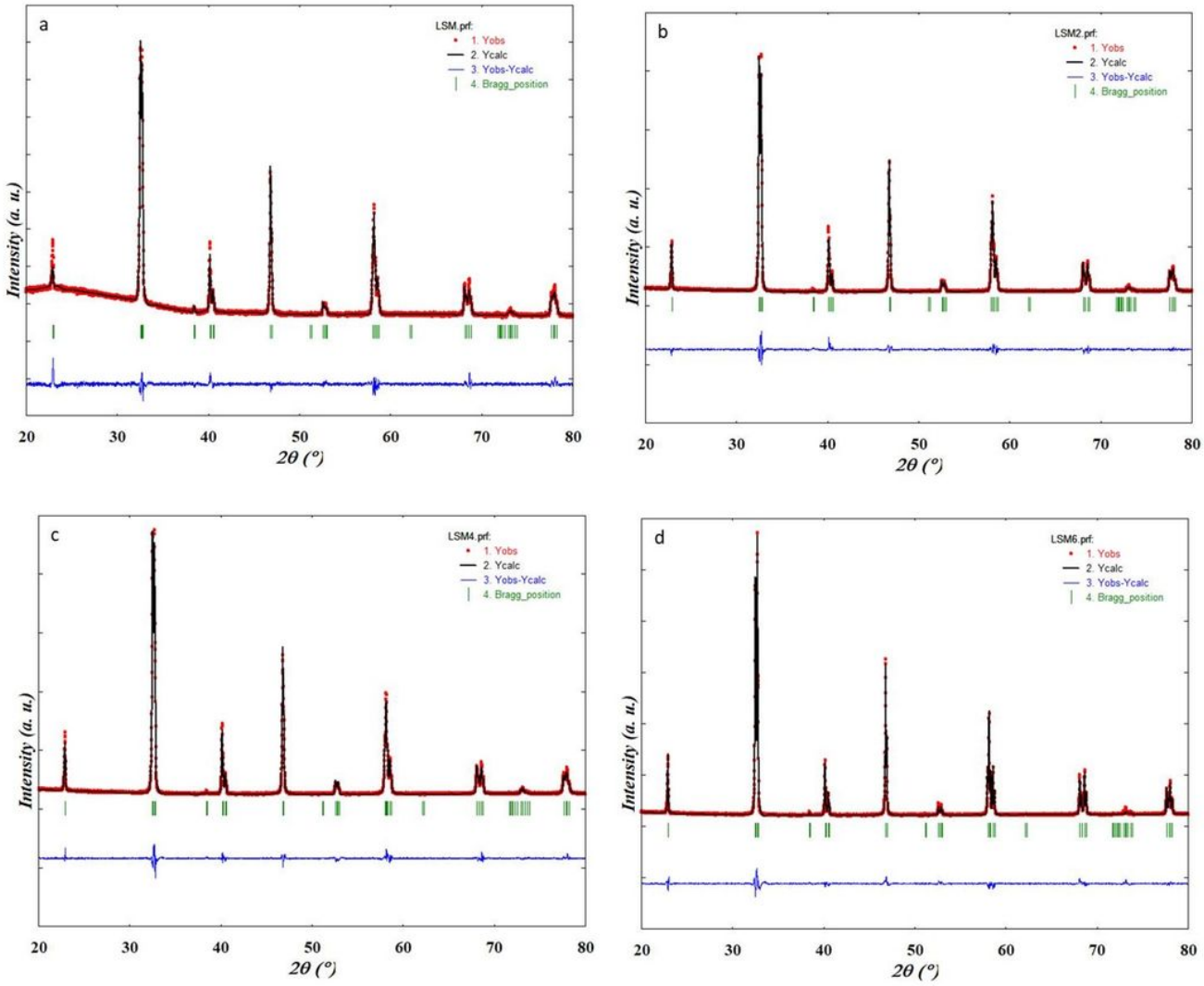


**Figure 1**

The XRD pattern of La0.7Sr0.3Mn1-xNixO3 (x = 0.00, 0.02, 0.04, 0.06) samples. The observed and calculated data are solid circle (red) and solid line (black) respectively. The blue line is the difference between the observed and calculated data. The positions of Bragg position reflection are represented by vertical green ticks.

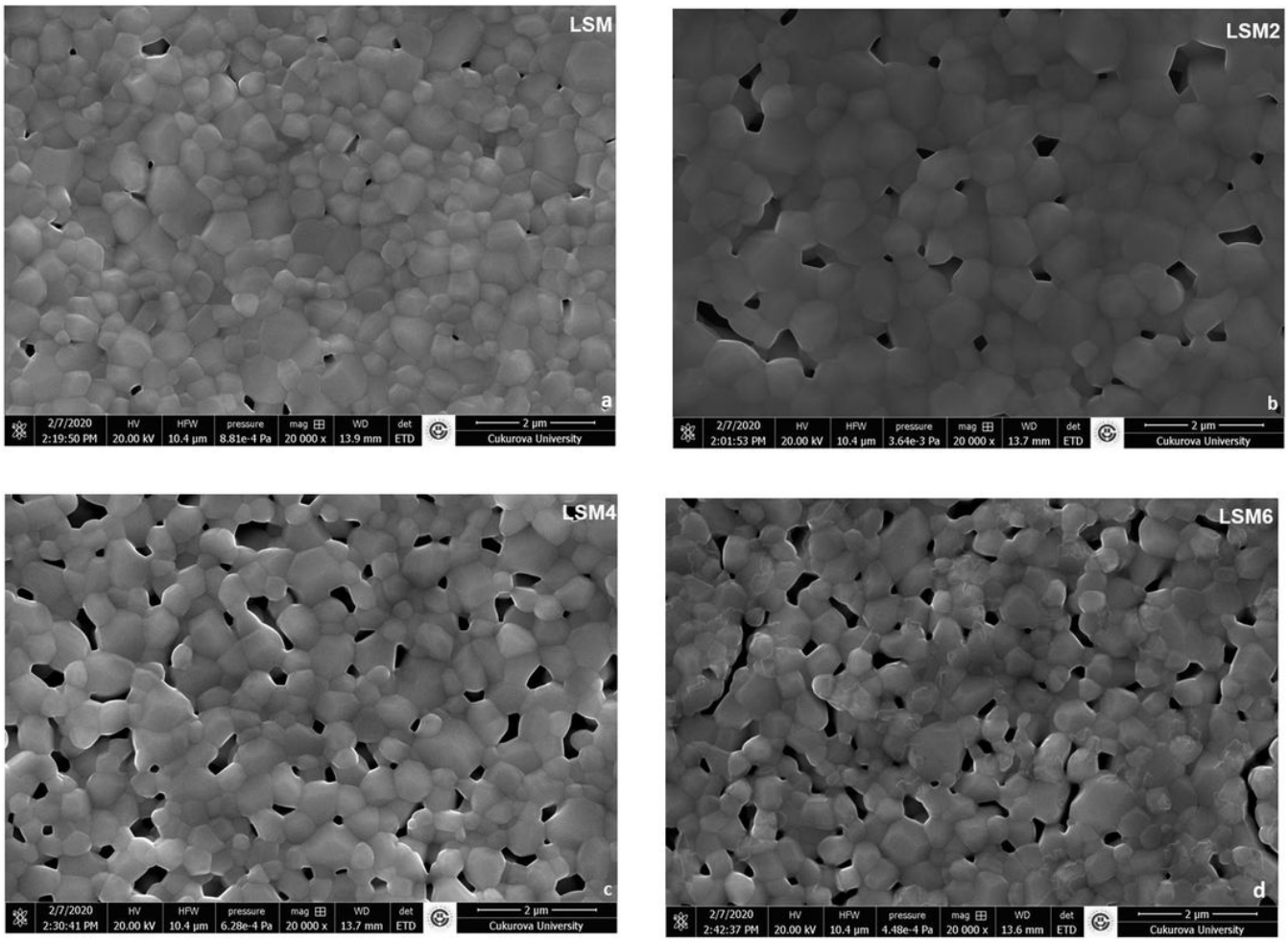


## Figure 2

SEM images of La0.7Sr0.3Mn1-xNixO3 (x = 0.00, 0.02, 0.04, 0.06) samples taken at 20 KX magnifications.

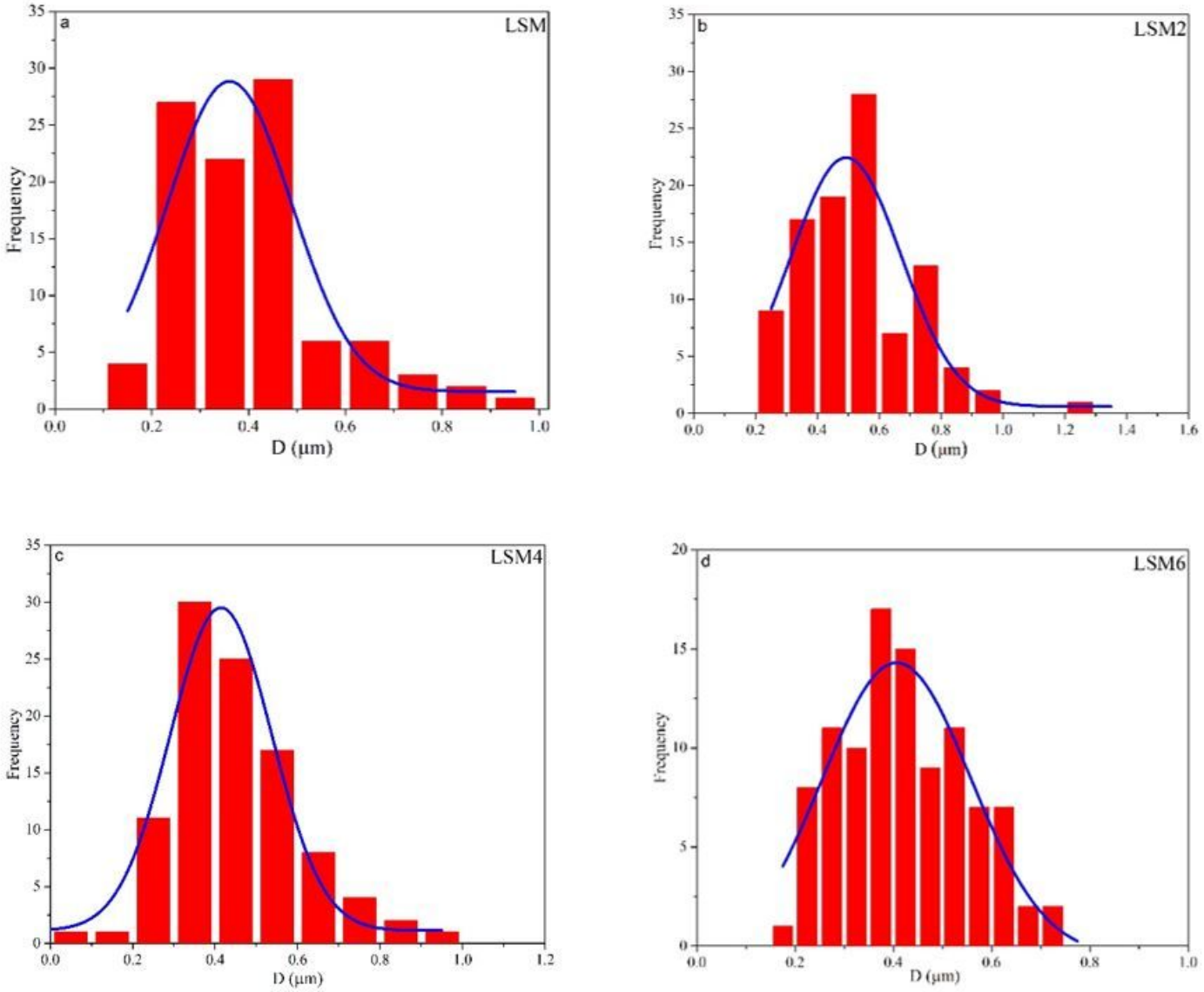


## Figure 3

The size distribution histogram of La0.7Sr0.3Mn1-xNixO3 (x = 0.00, 0.02, 0.04, 0.06) samples.

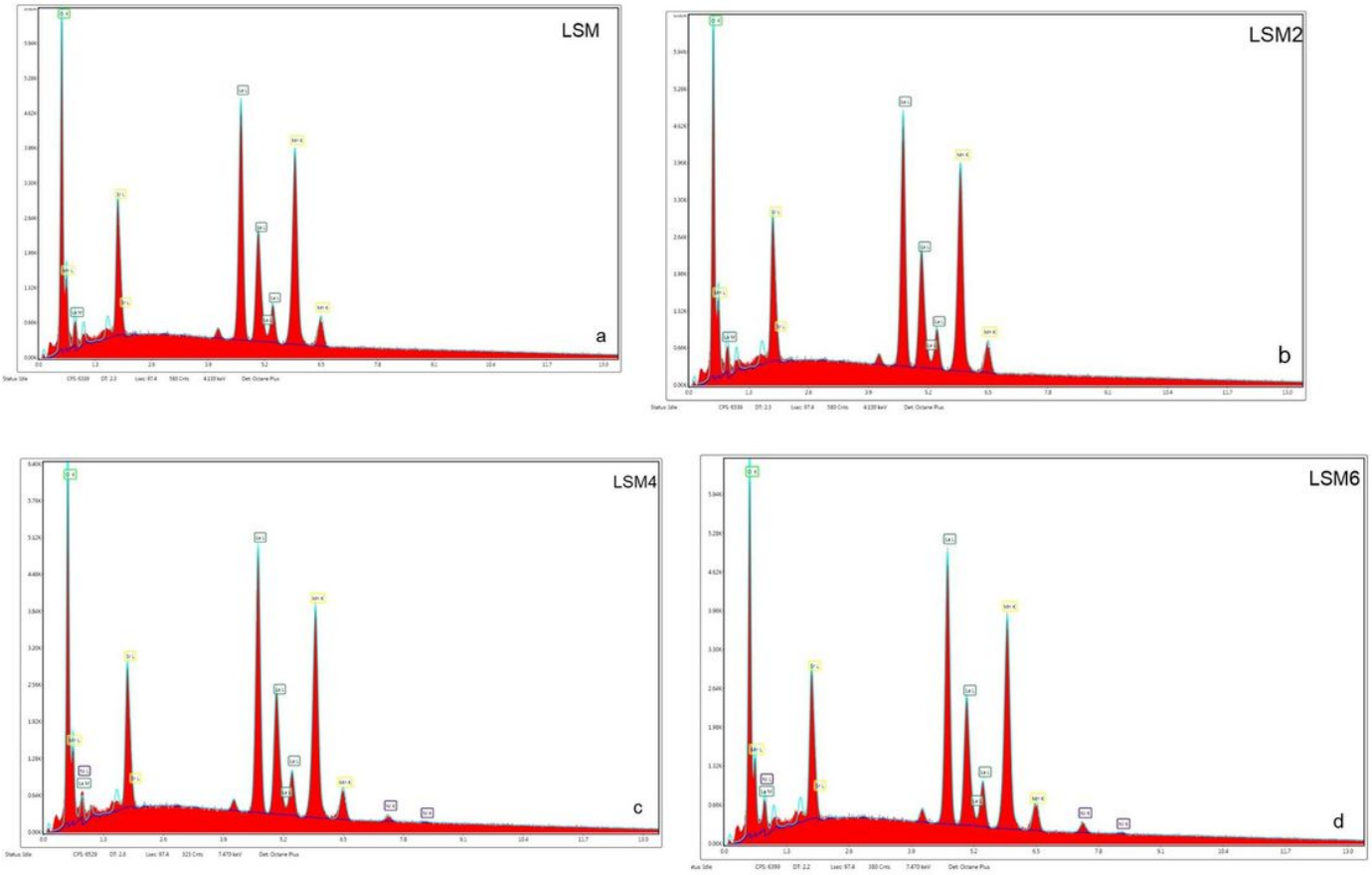


## Figure 4

EDS spectra of La0.7Sr0.3Mn1-xNixO3 (x = 0.00, 0.02, 0.04, 0.06) samples.

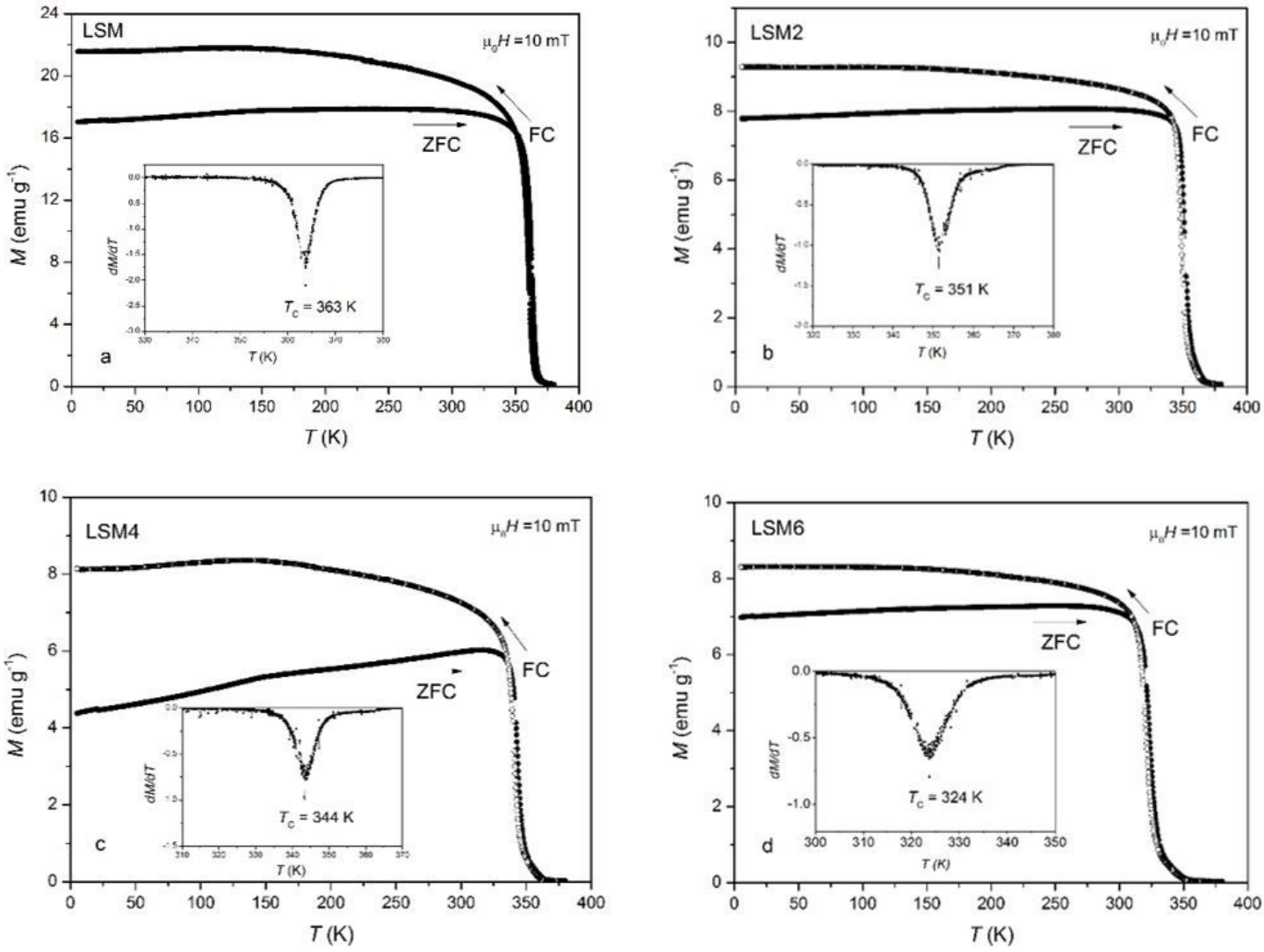


## Figure 5

M(T) curves of La0.7Sr0.3Mn1-xNixO3 (x = 0.00, 0.02, 0.04, 0.06) samples. Insets: Temperature dependence of dM/dT.

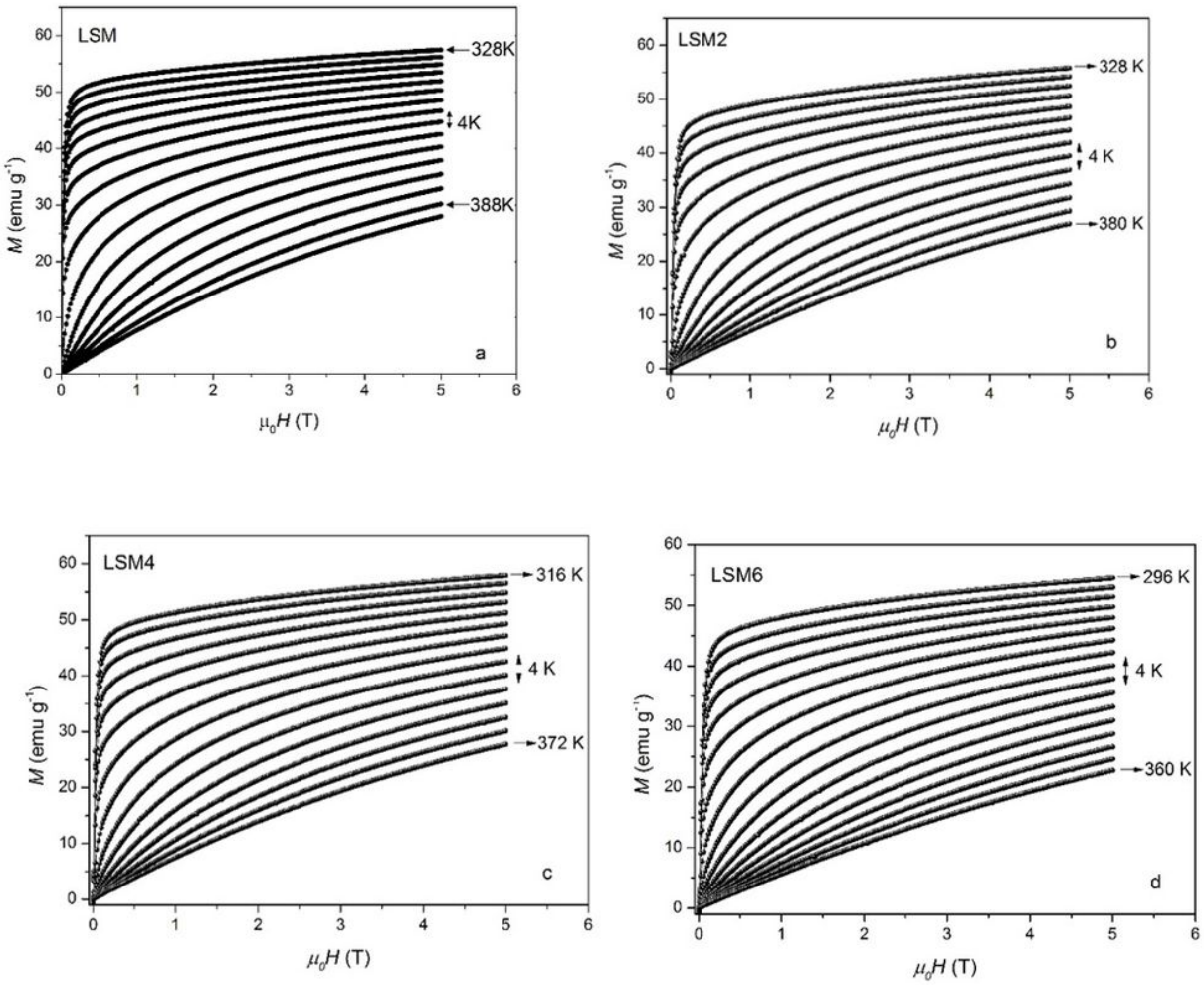


## Figure 6

M(H) curves of La0.7Sr0.3Mn1-xNixO3 (x = 0.00, 0.02, 0.04, 0.06) samples.

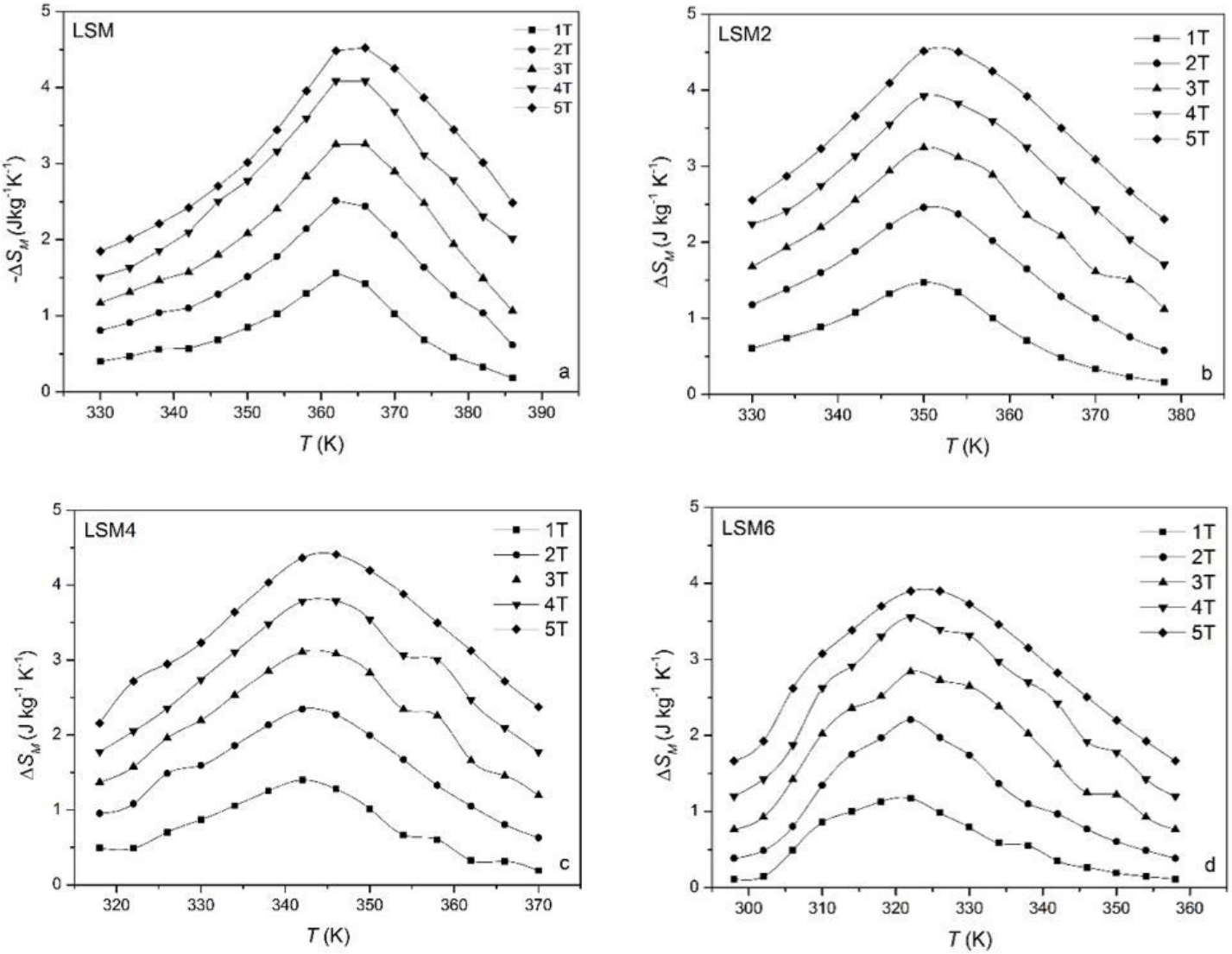


## Figure 7

ΔS_M (T) curves of La0.7Sr0.3Mn1-xNixO3 (x = 0.00, 0.02, 0.04, 0.06) samples at different applied magnetic fields.

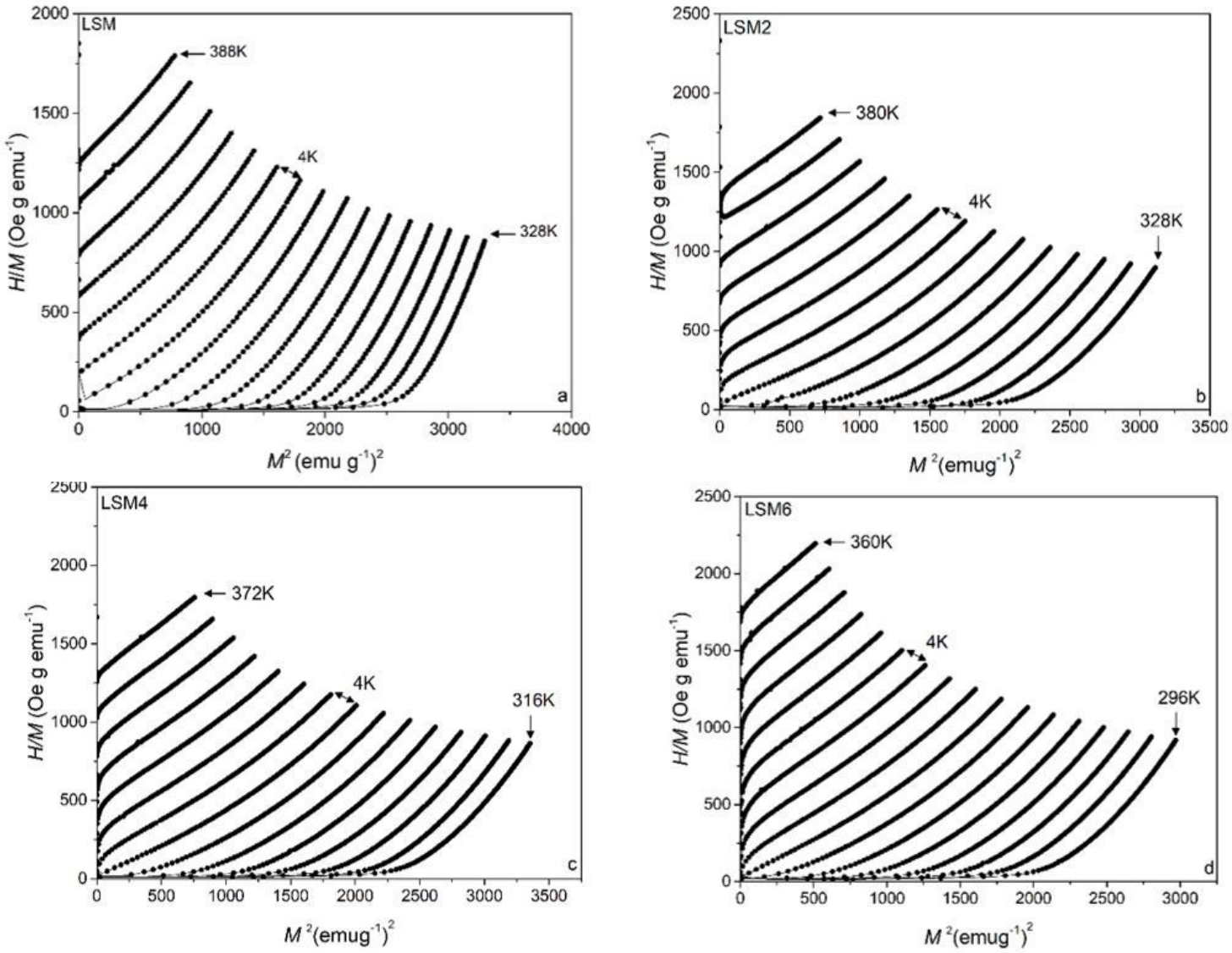


## Figure 8

Arrott plots of La0.7Sr0.3Mn1-xNixO3 (x = 0.00, 0.02, 0.04, 0.06) samples.

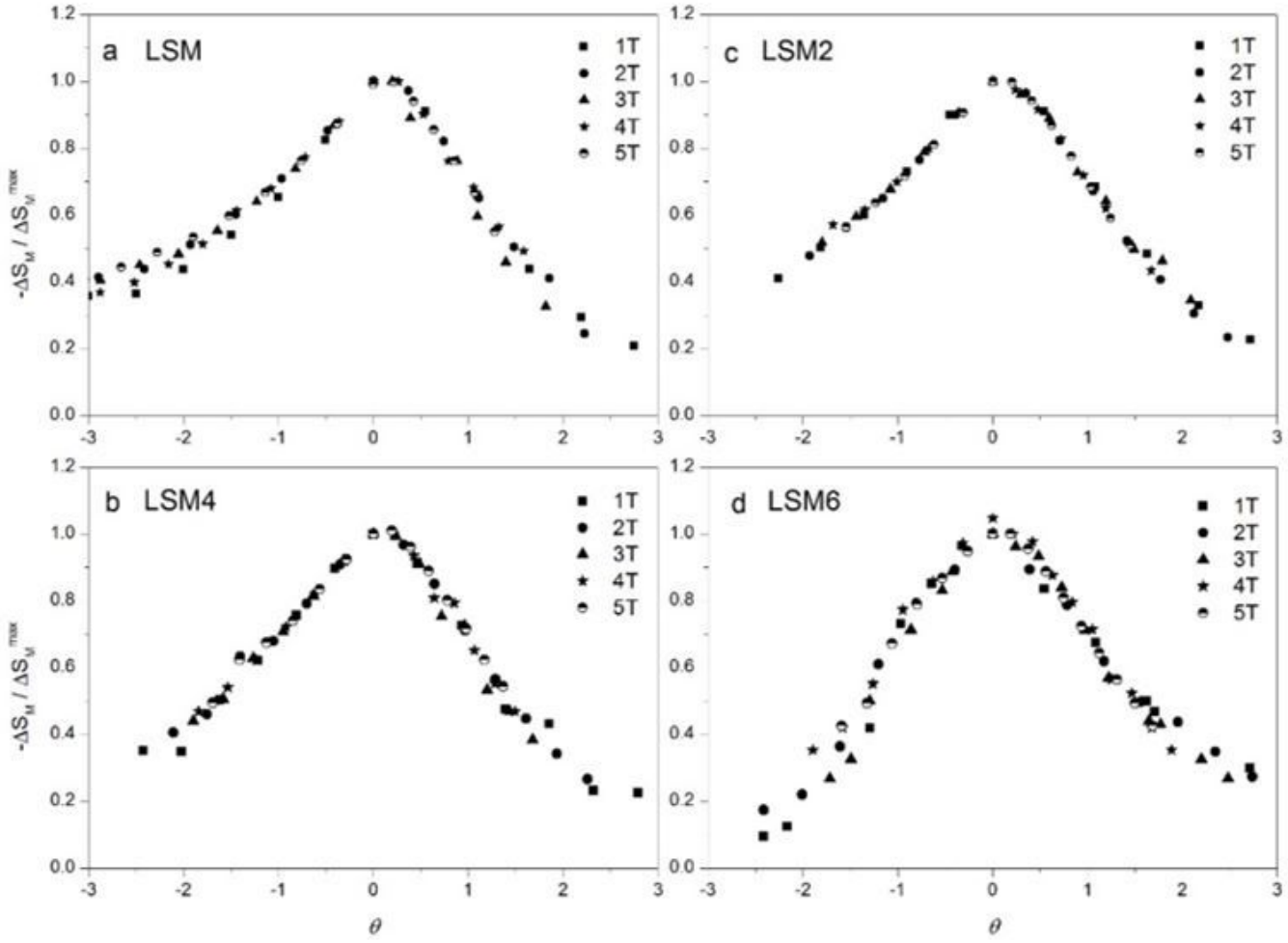


**Figure 9**

Rescaled temperature θ versus normalized magnetic entropy change curves at different magnetic field for La0.7Sr0.3Mn1-xNixO3 (x = 0.00, 0.02, 0.04, 0.06) samples.

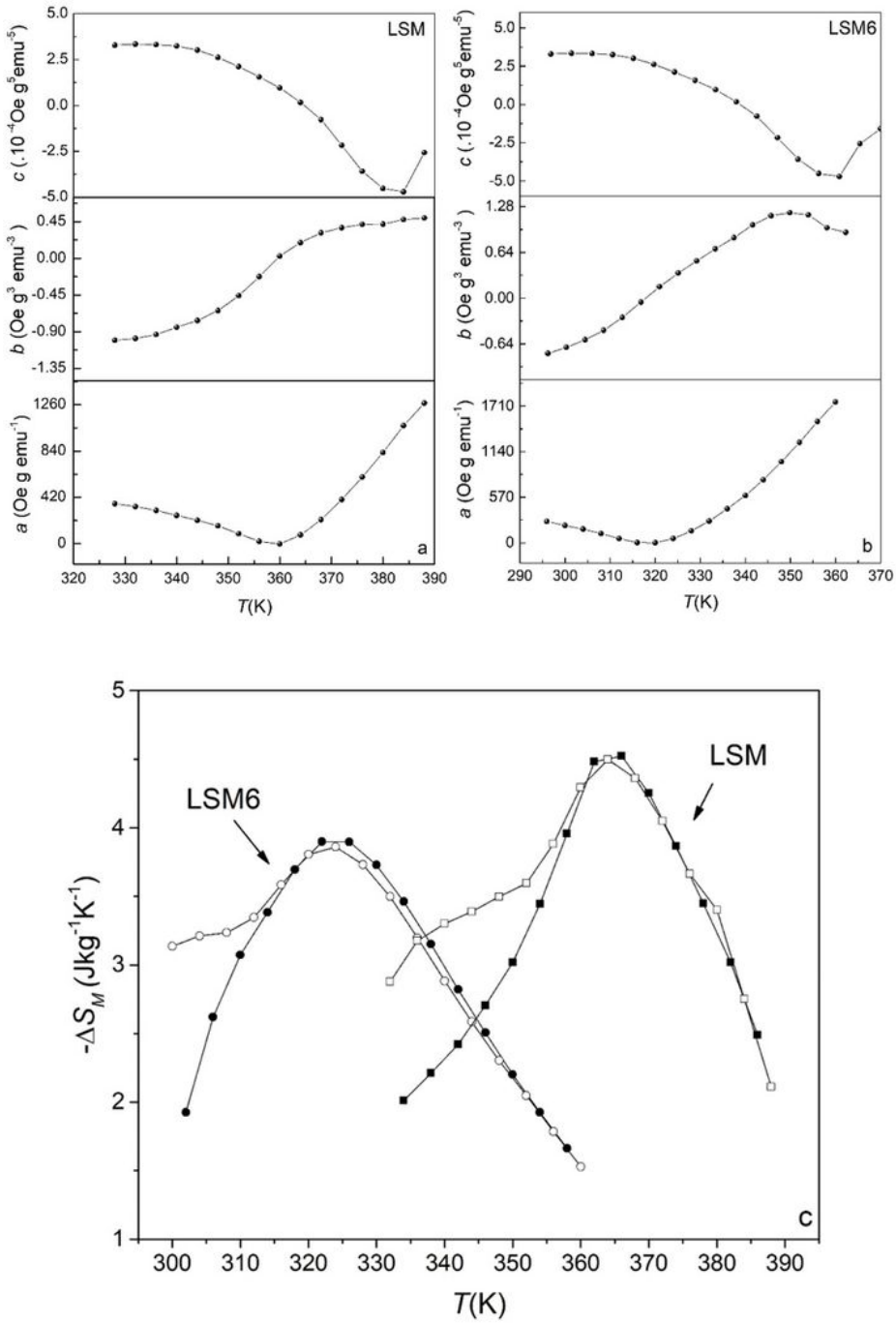


## Figure 10

The temperature dependence of the Landau coefficients for (a) LSM and (b) LSM6. The temperature dependence of the experimental and theoretical -ΔS_(M ) curves for LSM and LSM6 samples under magnetic field of 5 T.